Investigation of Thermal Properties of Blast Furnace Slag to Improve Process Energy Efficiency

By: Sara Yasipourtehrani

Submitted in fulfilment of the requirement for

The Master of Research

Environmental Science

Macquarie University

Australia

2016

Declaration

This thesis is a presentation of my original research work. Wherever contributions of others are involved, every effort is made to indicate this clearly, with due reference to the literature, and acknowledgement of collaborative research and discussions. The work was done under the guidance of Professor Vladimir Strezov, at the Macquarie University, Sydney, Australia.

Sara Yasipourtehrani

Abstract

Blast furnace slag (BFS) is the main by-product of iron making and is produced in large amounts worldwide. Analysing the properties of BFS, such as viscosity and heat exchange, at high-temperature conditions will help improve energy efficiency during the process. One of the steps in the iron making process is to heat the pig iron up to 1500°C for the next phase of steel-making. During this heating, a significant amount of energy is transferred to the BFS, and utilising some of this heat energy from the slag to contribute to heating pig iron would achieve energy efficiency. To improve energy usage, it is necessary to understand behaviour of the slags with differing compositions at varying temperatures. This knowledge is also important to assess the slag for further applications, such as use as concrete or cementitious material; however, the cooling process is known to have a significant effect on the end product properties and determine the end use of the slag. This study determines the thermal properties of selected slag samples using several in-situ experimental techniques. By comparing the chemical composition of the slags and their thermal behaviour, the effect of magnesium oxide and aluminium oxide was evident. Besides, the content of silicon dioxide had an effect on crystallization temperature and network strength.

Keywords

Slag viscosity, slag heat exchange, pig iron heating, slag behaviours, end use product value.

Abbreviations

- BF- Blast Furnace
- BFS- Blast Furnace Slag
- HS-SEM- Hot Stage Scanning Electron Microscope
- SEM- Scanning Electron Microscope
- EDS- Energy Dispersive Spectroscopy
- CATA- Computer Aided Thermal Analysis
- TGA- Thermogravimetric Analysis
- FTIR- Fourier Transfer Infrared
- GGBFS- Ground Granulated Blast Furnace Slag
- GHG- Green House Gas
- SCC- Self-compacting concrete
- SE- Secondary Electron
- BSE- Backscattered Electron
- PMT- Photon Multiplier Tube
- ICP-MS- Inductively Coupled Plasma Mass Spectrometry
- ICP-AES- Inductively Coupled Plasma Atomic Emission Spectrometry

Table of Contents

List of Figures

List of Tables

1. Introduction

Most metal extraction technologies pollute the environment with waste materials generated during the industrial process (Dippenaar 2005). These waste materials cause significant problems in terms of storage, transportation and environmental pollution (Ozturk & Gultekin 2015). In recent decades, industrialisation and urbanisation have increased rapidly, generating large amount of waste materials at a significant rate, where the existing landfill sites have filled rapidly, so the exploration of new sites is needed (Francis 2005). A critical issue of environment protection is the treatment of increased and diverse waste materials which threaten public health (Kuo et al. 2007). Because of landfill and environmental issues of increasing amounts of wastes, possible increased recycling of these materials or development of new by-products have become principal incentive for the industries (Francis 2005). The other area of interest for the industry is to increase processing efficiency, in terms of product output, quality and energy savings. This area of industrial processing is considered in the following section.

1.1. The Iron Making Process

The iron and steel making processes produce significant pollution and greenhouse gas emissions (Kan et al. 2015). Iron ore has different impurities and some of them, like aluminium, are the main structural constituents; while some, such as nickel, zinc and copper, are part of the trace element fraction (Kan et al. 2015). The target of this industry is to save natural resources by using waste materials and, where possible, conserve energy where material properties and characteristics are suitable (Motz & Geiseler 2001). Iron making also produces waste material which can potentially be recycled in a different industry (Motz & Geiseler 2001).

In the iron making industry, ore is placed in the blast furnace (BF) and, with the assistance of coke as a reductant and fuel, is reduced to molten metal as the final product of this process. The steelmaking furnace is further used for the production of the final steel product (Dippenaar 2005). Slag is a by-product of the iron and steel making process (Dippenaar 2005; Brodnax & Rochelle 2011). During iron and steel making, enormous amounts of slag are produced. The properties of different slags vary and are determined by the ore type and ash of the coke. The amount of steelmaking slag is less than the ironmaking slag (Dippenaar 2005). Slag can be considered as a renewable material that has not been used before, and the properties of this waste make its use possible in another part of the industry (Dimitrova 1995; Dippenaar 2005), which helps to reduce environmental contamination, energy use and production costs (Ozturk & Gultekin 2015). The possible reuses of BFS depend on the slag properties and heat

treatment of the molten slag. Therefore, it is necessary to enhance the knowledge of the phase chemistry of slag to optimise the productivity and performance (Jak & Hayes 2004). The development of new analytical equipment and application of new analyses will assist in improving the experimental methods (Jak & Hayes 2004).

Molten slag is the major component of the process, and it is important to understand its thermophysical properties to obtain the maximum performance. The slag composition is known to affect the microstructure and its thermophysical properties (Kang et al. 2014). Blast furnace slag (BFS) largely consists of Al_2O_3, SiO_2, CaO, and MgO as main components with other compounds like TiO, FeO, and MnO_2 present in small amounts (Francis 2005; Ozturk & Gultekin 2015).

BFS is produced in the largest amounts in the initial iron making (Gan & Lai 2014). When producing 1 tonne of pig iron, 300 kg BFS is produced (Fredericci et al. 2000). Worldwide, BFS is manufactured in significant amounts estimated at 175-225 million tonnes per year (Savastano et al. 2001; Francis 2005). The function of the BF is to separate gangue, and non-metallic impurities from the iron ore with the final products being pig iron and slag (Dippenaar 2005). Pig iron and molten slag accumulate at the hearth of the BF, and the slag is positioned above the pig iron, as its density is lower than iron (Ito et al. 2014). BFS segregates from the pig iron during the production process (Crossin 2015). Figure 1 demonstrates a cross-section of a commercial BF. It is hard to drain the slag from the BF as it has high viscosity and in the lower temperature zones of the furnace this viscosity increases (Ito et al. 2014).

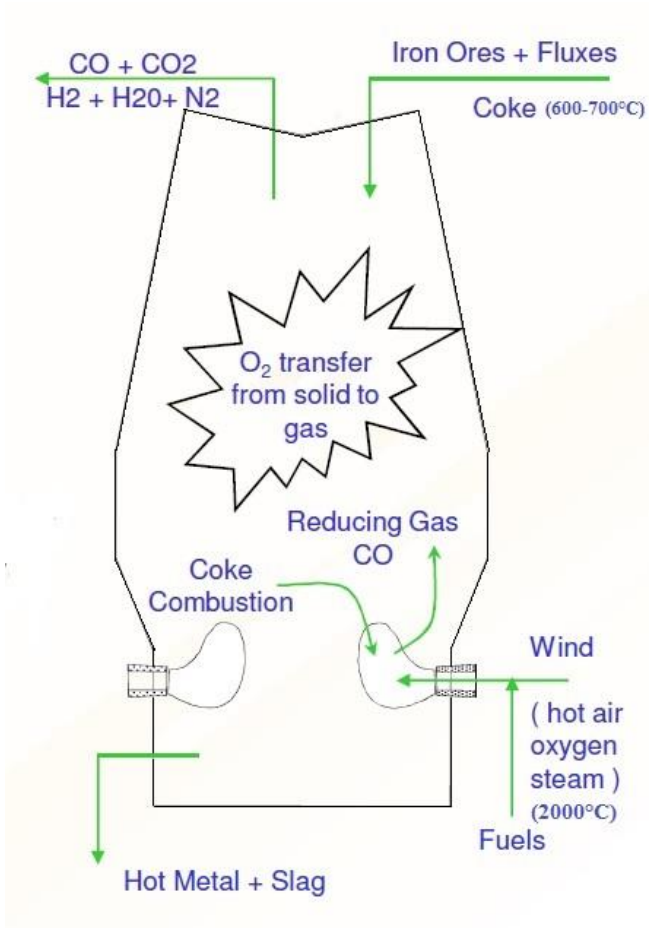

Figure 1- A functional cross section of a traditional BF

When slag is tapped from the furnace it has a high temperature and different methods of cooling will affect its composition (Dippenaar 2005). The slag has particular characteristics, such as high strength and hardness, that make it valuable in several applications (Fredericci et al. 2000). Appropriate treatment of high-temperature slag with a suitable cooling process improves the slag properties and its applications for recycling in other parts of the industry (Liapis & Papayianni 2015).

The use of BFS in building material production, like concrete and cement, has various benefits (Ozturk & Gultekin 2015). The final product can be additionally crushed and used as road construction base material (Barati et al. 2011). Moreover, ferrous slag contains high amounts of calcium silicate and can be used as cementitious material (Barati et al. 2011). BFS could be also utilised in the glass and ceramic production (Francis 2005). The chemical and mechanical properties of glass-ceramic, which is produced from slag, make a high-quality product (Wang et al. 2010). However, inappropriate cooling of the slag causes the physical properties to become weak, which thus restricts the reuse of slag in other industries, such as cementitious material and concrete (Barati et al. 2011; Liapis & Papayianni 2015). Chemical

properties and the cooling rate of solidification affect the mineralogy and hydraulic properties of slag (Kriskova et al. 2013). Table 1 demonstrates the most important type of slag as a by-product and the end use of these materials. BFSs can be divided into two types of slags, the rapid cooling and slow cooling slag, each offering different possible reuse options in other suitable applications (National Slag Association 2013; U.S Geological Survey 2014).

Table 1- Potential slag by- products and uses

Slag By-Products	Slag Uses
Crystalline Phase (Slow Cooling)	Road base, ready-mix concrete, clinker manufacture, asphaltic concrete aggregate, fill, railroad ballast, hot mix asphalt, concrete pavement, concrete base, prevent erosion in the slope,
Amorphous Phase (Rapid Cooling)	Concrete, cementitious additive, can be mixed with Portland cement clinker to make a blended Type 1S cement, high fire-rated concrete base, lightweight fill applications over edgy soils,

The hypothesis of this thesis is to investigate the thermal properties of BFS and explore how to use the heat energy of BFS in heating the pig iron. It is essential to prepare the pig iron for the next step, which is the steel making process, while maintaining the value of BFS as a base material for other applications, such as concrete, cement, road construction, cementitious material or higher valuable materials.

1.2. Thesis structure

In this Thesis, Hot Stage Scanning Electron Microscope (HS-SEM), Energy Dispersive Spectroscopy (EDS), Computer Aided Thermal Analysis (CATA), Thermogravimetric Analysis (TGA), and Fourier Transform Infrared (FTIR) Spectroscopy were used as a part of the experimental analysis of BFS properties. The SimaPro is a software that was used for analysing the possibilities of reuse of slag on the practical scale. In Chapter 2, the most relevant literate will be reviewed to address the thesis question. In Chapter 3, the details of methodology, which was used in this research, are explained. In Chapter 4, the results and discussions are elaborated. In the last chapter, the conclusion and recommendation are clarified.

2. Literature Review

BFS has different behaviour under different conditions, so it is important to understand these conditions and the slag's responses, such as cooling process, basicity ratio, eutectic point, the microstructure of BFS, energy efficiency, viscosity, melting point and heat exchange. In the following paragraphs, each of these properties is reviewed in more detail.

2.1. Slag Properties

2.1.1. The Cooling Process

The chemical content and the cooling rate affect the mineralogy and hydraulic properties of the slag (Kriskova et al. 2013). When slag tapped from the furnace has a temperature of about 1480ºC, and is subjected to different methods of cooling, such as rapid or slow cooling, it affects the slag properties (Dippenaar 2005). Molten slag has two separate final solid states. The first one is the crystalline phase, which comes from the slow cooling of the molten slag (Bisio 1997; Jak & Hayes 2004; Dippenaar 2005; Kuo et al. 2007; Kriskova et al. 2013). The second one is a glassy, amorphous or vitreous phase, which is caused by quenching or rapid cooling (Bisio 1997; Jak & Hayes 2004; Dippenaar 2005; Kuo et al. 2007; Kriskova et al. 2013).

In preparing the glassy or amorphous phase, there are two ways of quenching, including wet quenching and dry quenching (Barati et al. 2011). In wet quenching, water is used to cool the slag quickly (Barati et al. 2011; Kriskova et al. 2013). An enormous amount of water, about 1-1.5 tonnes of water for every 1 tonne molten slag, is required (Barati et al. 2011; Kriskova et al. 2013). The water quenching technique produces granulated BFS (Crossin 2015). Slag causes environmental pollution when it is poured into the slag pit with the usage of water for quenching, because the H_2S and SO_2 are produced and released into the water and atmosphere (Bisio 1997; Barati et al. 2011). The dry quenching method is used as a way to recover the heat energy of the molten slag in the form of hot air, steam, or chemical energy (Barati et al. 2011).

Water is more efficient for cooling in comparison with air, as it drops the average temperature faster (Kriskova et al. 2013). The size and thickness of the cooled material also have an effect on the overall cooling rate (Kriskova et al. 2013). Inappropriate cooling causes the physical properties to become poor and restrict reuse of slag (Liapis & Papayianni 2015). Quenched slag could be used as railroad ballast, in concrete and in Portland cement (Dippenaar 2005). The air-cooling technique is applied for a lower-

value applications, such as the production of bitumen (Crossin 2015). Appropriate treatment of slag with high-temperature and suitable cooling process increases the slag properties and the value of its applications (Liapis & Papayianni 2015).

2.1.2. Basicity

The ratio of CaO to SiO_2, which is called basicity, is critical to the slag characterisation (Kuo et al. 2007) as this ratio affects the crystallisation (Kuo et al. 2007). If the CaO to SiO_2 ratio is >0.99 the crystalline phases will appear, and the crystallisation will not be related to the cooling process. If the basicity ratio is <0.674, the water quenching will enhance the amorphous phases (Kuo et al. 2007).

2.1.3. Eutectic Point

An equilibrium of liquids and solids occurs during rapid cooling (Jak & Hayes 2004). The eutectic point is the temperature at which all liquids change to their solid phase. The composition might change during heating because some components may disappear due to evaporation or reaction with contaminant elements (Jak & Hayes 2004). Segregation is a process which lets physical segregation of liquid and solid occur at temperatures below the melting point. This segregation will affect the fluidity of slag due to the appearance of solid phase and increase the viscosity.

2.1.4. Microstructure of BFS

There are different crystalline phases for BFS after heat treatment, such as: merwinite, melilite, larnite, gehlenite, and åkermanite (Fredericci et al. 2000). Merwinite (Ca_3 Mg $(SiO_4)_2$) is a metastable phase of BFS, and it forms at 1000°C (Fredericci et al. 2000). By further heating, merwinite irreversibly disappears to the thermodynamically stable phase (Fredericci et al. 2000). Melilite, which is another crystalline phase, includes all principal components of BFS and 10wt% Al_2O_3 (Fredericci et al. 2000). Larnite (Ca_2SiO_4) is a slag with more SiO_2 and CaO than is needed to form åkermanite ($2CaO.MgO.2SiO_2$) and gehlenite ($2CaO.\ Al_2O_3.SiO_2$), which are known as the melilite series (Fredericci et al. 2000). Melilite is a solid solution between gehlenite and akermanite (Fredericci et al. 2000). The excess CaO and SiO_2 is sufficient to form calcium silicate (Fredericci et al. 2000). In the Slag Atlas, the different phases of BFS microstructures are shown as a resource according to their chemical compositions, so it is possible to recognise the microstructure of the BFS samples by comparing the image obtained in the investigations with the Slag Atlas (Eisenhuttenleute 1995). The temperature of crystallization affects the crystalline phase, such as gehlenite, diopside pyroxene and barium aluminium

silicate (Wang et al. 2010). For instance, the diopside phase (CaMg (Si, Al, Fe)$_2$ O$_6$) is formed at 1120°C (Wang et al. 2010). Figure 2 demonstrates different characteristic compositions of BFS in two systems of CaO-SiO$_2$-Al$_2$O$_3$ and CaO-SiO$_2$-MgO according to the Slag Atlas (Eisenhuttenleute 1995). Melilite is a solid solution of åkermanite (Ca$_2$MgSi$_2$O$_7$) and gehlenite (Ca$_2$Al$_2$SiO$_7$) (Mendybaev et al. 2006). They have a temperature-composition relationship (Mendybaev et al. 2006). Melilite consists of åkermanite and gehlenite and produces interrupted solid solution (Mendybaev et al. 2006). Every sample shows different behaviour at different temperatures and this is related to the chemical content of the sample (Mendybaev et al. 2006). According to Figure 3, when the amount of Al$_2$O$_3$ increases the gehlenite phase will be obtained, but when the amount of MgO is increased the åkermanite phase will be obtained (Mendybaev et al. 2006).

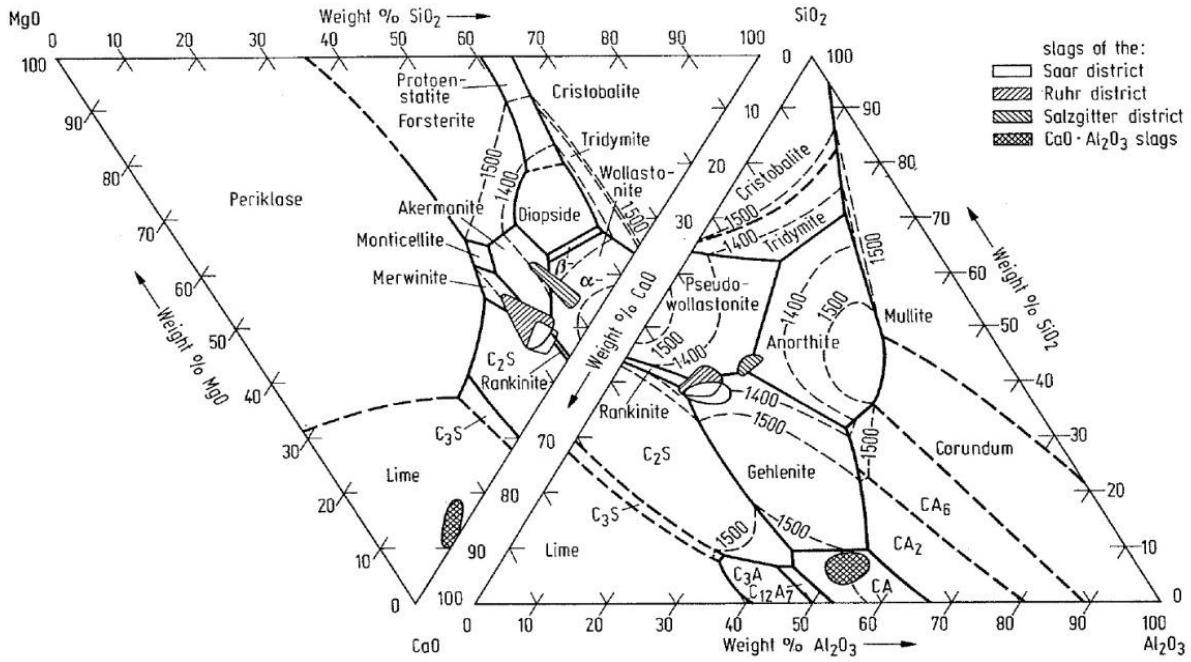

Figure 2- The characteristic composition of BFS according to the Slag Atlas (Eisenhuttenleute 1995).

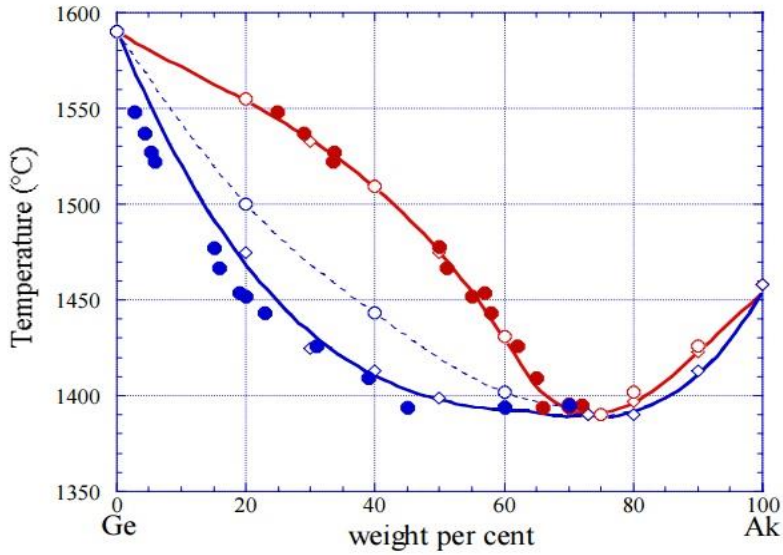

Figure 3- Melilite is a composite of gehlenite and åkermanite. The red curve depicts the liquid relationship, and the blue curve is for solids (Mendybaev et al. 2006).

2.1.5. Energy Efficiency

Significant energy exists in the molten slag that is tapped from the BF, and this can be used for conserving energy consumption (Bisio 1997; Barati et al. 2011). BFS has a high temperature of 1450-1650°C which is a valuable energy potential; however, significant amount of energy (near 220 TWh/year) is wasted because cooling is usually done without the energy being recovered (Bisio 1997; Barati et al. 2011). The logical and best way for using recovered energy is to use it in the same BF and avoid transportation over long distances (Bisio 1997).

There have been many attempts to recover the energy from slag for use as heat, electricity generation or fuel, but none of them has been commercialised yet (Barati et al. 2011). The reason for this is that this industry is more focused on quenching the slag and having the glassy phases rather than recovering the energy (Barati et al. 2011). All of the BFS is sold as a raw material for other products or processes (Bisio 1997). To keep the value of the slag, rapid cooling is vital (Bisio 1997). If recovery of energy is the goal, the slag is not cooled fast enough to manufacture the glassy phases (Barati et al. 2011).

2.1.6. Viscosity

Viscosity is an important property which shows movement and fluidity of slag during the process (Togobitskaya et al. 2004). The viscosity at different temperatures determines surface tension and fluidity

of the BFS (Togobitskaya et al. 2004); the viscosity of molten slag changes with the chemical composition and temperature (Saito et al. 2003; Gan & Lai 2014). Viscosity is an important physical property to understand the network structure of molten slag and to simulate the different phenomena at various temperatures, and viscosity has an additional effect on transportation of slag (Saito et al. 2003; Gan & Lai 2014).

It is vital to investigate the relationship between slag composition and viscosity (Kim et al. 2004). If the slag is cooled, the solid phases will appear and increase the viscosity (Kim et al. 2004). The composition of phases will change continually when the temperature is reduced from liquid to solid. The crystallisation of molten slag is also related to the viscosity (Zheng et al. 2014). According to the experiment by Kim et al. (2004), MgO did not have a significant effect on slag's viscosity if the amount of Al_2O_3 was fixed. However, increasing MgO up to 12.5% will enhance the mobility of slag (Logachev et al. 2013). Logachev et al. (2013) concluded that if the content of MgO increases to 12.5% and the basicity is between 0.94 and 1 the slag mobility could be increased, even with a high content of Al_2O_3.

The viscosity of molten slag increases with reduced temperature and this phenomenon causes difficulties in the industry (Nakamoto et al. 2004). Thus, maintaining or increasing the fluidity of molten slag in low temperatures should be investigated to achieve the best operation and save energy (Nakamoto et al. 2004). The viscosity is low if the CaO/SiO_2 ratio is high (Nakamoto et al. 2004). For having an adequate slag system with low viscosity and low temperature, the reaction of a wide range of slags with differing chemical compositions should be examined (Nakamoto et al. 2004). For instance, according to Nakamoto et al. (2004) the viscosity of BFS, with particular composition, enhances at temperatures lower than 1673°C. This temperature is when BFS is in a liquid state, while at temperatures below 1673°C liquid and solids coexist (Nakamoto et al. 2004). The viscosity of molten BFS should be less than 0.6 Pa·s to have a manageable fluidity (Nakamoto et al. 2004). The viscosity of slag at 1673°C is 0.77 Pa·s as reported by Nakamoto et al. (2004), which shows that this slag does not have a suitable fluidity at that temperature. It is important to understand the physical properties of slag at high temperatures for obtaining higher efficiency, lower cost and insight into the dynamic and structure of slag (Gan & Lai 2014).

2.1.7. Melting Point

The melting point is one of the critical properties of BFS that is related to the chemical content. The slag conductivity depends on viscosity, which means that it depends on slag microstructure (Kang et al. 2014). The thermal conductivity is reduced at the melting point of the molten slag, because the amount of non-bridging oxygen ions is increased (Kang et al. 2014). In a variety of experiments, the effects of some chemical composition, such as Al_2O_3, MgO and basicity (CaO/SiO_2 ratio), were studied in the past. Liang et al. (2011) concluded that Al_2O_3 could rapidly decrease the melting point of the BFS. Lee et al. (2004) found that FeO is another component which reduces the melting point of slag with increasing the FeO content. Additionally, MgO at less than 7% works as a network modifier in BFS composition, while amounts above 7% MgO cause an increase in BFS melting point (Lee et al. 2004; Kim et al. 2004). The BFS melting point and liquid temperature increases by increase in the basicity ratio (Lee et al. 2004; Dai & Zahang 2012). The high amount of SiO_2 reduces the melting point and retards formation of crystals in the slag, increasing the strength and water permeability. SiO_2 also controls the calcium leaching in the slag (Kuo et al. 2007; Nazari & Riahi 2011). According to Kim et al. (2004) the liquid temperature of BFS with a basicity of 1.45 and 14% Al_2O_3, decreases with the increase in the amount of MgO content. Increasing the amount of MgO from 3.5 to 10% increases the melting point of slag when the content of Al_2O_3 is 14% (Kim et al. 2004).

2.1.8. Heat Exchange

Most of the heat exchange occurs in the BF hearth affecting the quality of the metal, productivity of the furnace and operating parameters (Formoso et al. 1999). All the processes occurring in the BF are concerned with heat exchange, between the descending material and ascending hot gasses, as demonstrated in Figure 1. To increase furnace efficiency, more heat power is needed for heating the pig iron and slag. The heat and energy exchange occurs in the raceway of a BF. Although the raceway has 1% of the inner volume of the BF, it has an essential function in heat and energy exchange in the ironmaking industry (Formoso et al. 1999). Radiation from the raceway has the primary role of heating the pig iron and slag in the liquid bath of the hearth. Thus, the raceway exchanges the heat in the liquid product from melting.

2.2. Slag Composition and End Use

2.2.1. Concrete and Cementous Products

The concrete industry has an enormous environmental footprint. Concrete is used as a building material and on a commercial scale 10 billion tonnes of concrete is produced every year (Meyer 2009) requiring massive amounts of raw materials and energy for production. Thus, the concrete industry is neither environmentally friendly nor sustainable (Meyer 2009). The reasons for its extensive use are excellent mechanical and durability characteristics in suitable design and production. Concrete is mouldable, has variable fire resistance and is an available and affordable material. However, the effect of this industry on the environment is unavoidable. The natural resources, required for this industry, are enormous using large amount of water and energy during the process. Finally, destruction and disposal of cement and concrete products, after use, cause other environmental issues (Meyer 2009).

Most of these problems and difficulties are caused by the need for Portland cement which is an essential part of concrete manufacturing. If the demands for Portland cement is reduced, the environmental destruction will also reduce. CO_2 emissions increase during Portland cement production, but cementitious materials are a good substitute for Portland cement, and some of those materials are wastes from industrial processes, such as fly ash or ground granulated blast furnace slag (GGBFS) (Meyer 2009). To produce 1 tonne of Portland cement another tonne of CO_2 is released into the atmosphere, and worldwide 7% of all CO_2 is generated by this industry (Meyer 2009). GGBFS is the glassy granulated material which is formed from molten BFS that is rapidly cooled (Meyer 2009). The slag is regularly substituted for cement up to about 50% and sometimes 70-80% (Meyer 2009). Slag improves the chemical stability and strength of concrete and also reduces the heat of hydration (Meyer 2009). The aim of the concrete industry is to replace Portland cement as much as possible, with other cementitious materials, especially the waste materials of other industries.

Supplementary cementitious materials currently used in the concrete blends include fly ash, silica fume, steel slag and GGBFS (Crossin 2015). When the use of GGBFS is not restricted the emissions of greenhouse gases reduce by about 47.5% (Crossin 2015). However, the use of GGBFS in the concrete blend is constrained, so it is not possible to achieve the 47.5% reduction in the greenhouse gas emissions (Crossin 2015). The reason of this constraint is related to the slow hydration rate of BFS and low compressive strength of BFS at the early age (Menendez et al. 2003). Addition of limestone will solve the issue of early strength of BFS, and the later strength of BFS will be improved by purifying the pore with cementing materials (Menendez et al. 2003). CO_2 comes from the fossil fuel combustion which is

used for calcination of $CaCO_3$ to CaO, mineral production and transportation (Crossin 2015). Concrete is used in vast amounts as a construction material and statistics show that every person uses 3-3.8 tonnes of concrete produced in the world each year (Crossin 2015). One potential strategy for reducing the greenhouse gas emissions is to use as much GGBFS as possible instead of Portland cement, in concrete production. By using GGBFS in concrete manufacture, the Green House Gas (GHG) emission can be reduced by 22-40% (Crossin 2015). But it is important to calculate the emissions which come from processing and transporting GGBFS. However, as BFS is a waste material its contribution is excluded (Crossin 2015).

GGBFS is already highly utilised in cement and the concrete applications, especially for high-performance concrete (Wan et al. 2004). The main reason for using GGBFS is its shape and micro-aggregate effect (Wan et al. 2004). Also, the grinding methodology will affect the characterization of GGBFS (Wan et al. 2004). Fine grinding enhances the surface area and this will improve the mechanical activation (Kumar et al. 2008). When the mechanical reactivity is increased, the strength of concrete and cement will be improved (Kumar et al. 2008).

The stability and chemical durability of slag are important as it is used in building materials as well as paving (Kuo et al. 2007); and GGBFS could replace as much as 35-65% of Portland cement in production of concrete (Nazari & Riahi 2011). If we replace Portland cement with GGBFS, the emission of CO_2 will reduce and the amount of this replacement have an effect on CO_2 emission (Nazari & Riahi 2011). Moreover, energy is saved as the grinding of slag uses only 25% of energy needed for manufacturing Portland cement (Nazari & Riahi 2011).

When GGBFS, which has a high amount of SiO_2, is used instead of Portland cement in the process of concrete manufacturing, the strength and water permeability of concrete will increase (Nazari & Riahi 2011). Using GGBFS to about 45wt% is beneficial for increasing the tensile strength of concrete (Nazari & Riahi 2011). More than this amount is not appropriate since the amount of CaO is reduced, but is required in the concrete structure (Nazari & Riahi 2011).

Self-compacting concrete (SCC) is a high efficient concrete with excellent rheological properties and valuable segregation resistance (Zhao et al. 2015). By using SCC, the construction time and cost is reduced (Zhao et al. 2015). Also, the vibration and noise are diminished during the process (Zhao et al. 2015). However, Ordinary Portland Cement is needed for producing SCC but is expensive and generates CO_2, so it does not meet the economical and environmental requirements (Zhao et al. 2015). To solve

this problem, the use of by-product materials, such as fly ash and GGBFS, are recommended (Zhao et al. 2015). The annual worldwide production of fly ash and GGBFS is 450 million tonnes and 530 million tonnes respectively (Zhao et al. 2015). Consequently, if fly ash and GGBFS are used to replace cement in the production of SCC, the emission of CO_2 can be reduced (Zhao et al. 2015). By re-using by-products of other industrial activities, the cost of operation is also diminished (Zhao et al. 2015).

The most relevant literature was reviewed here for understanding the difficulties and the purposes of this study. Initially, slag has the high temperature when it is tapped from the BF and the first purpose of this study is to use this energy for heating the pig iron. The pig iron should be heated up to 1500°C for the steel making industry. Another important purpose is to keep the slag value for the end use or recycling purposes. For doing this, it is essential to quench the BFS; however, the quenching of BFS does not let us use the heat energy.

The overall aim of this study is to determine the properties of blast furnace slag samples to exchange the heat energy between slag and pig iron into the hearth of BF while quenching the slag for keeping the value of it for future use. The first aim is to compare their melting points and chemical contents of slag for finding the relationship between chemical compounds and melting points of BFS to determine which elements have the most significant effect on melting points of the samples. The second aim is to determine the crystallization behaviour of the samples according to their chemical contents and observe the crystal compositions, the reactions and interactions of these three samples in different temperature, which will show the effect of chemical composition on their behaviour. The third aim is to investigate the endothermic or exothermic effect of samples in different temperature and try to figure out the mechanisms for these reactions. All these data, will help us to understand the thermal behaviour of samples and the reasons of these behaviours, so it will be easier for us to find the way for our purpose which improving the heat energy efficiency of BFS to heat the pig iron while quenching the BFS. This heat exchange is related to the viscosity of slag and viscosity is related to the chemical content of BFS and its crystallization behaviour.

3. Materials and Methods

3.1. Sample and Preparation

The samples used in this study were BFS supplied from China. The samples were quenched after the heating process, and this resulted in the amorphous and glassy phases of the sample (Figure 4). The samples were not uniform in structure due to differing speeds of solidification between the surface and inside the molten slag. For minimizing variability, samples were ground into a fine powder and mixed to form homogeneous sub-samples. A Standard Ring Mill batch pulverizer (ROCKLAB SARSD) was used to grind the sample to fine powder. The particle size distribution after grinding for each sample was between 10 and 100 µm determined with SEM imaging (Figure 5).

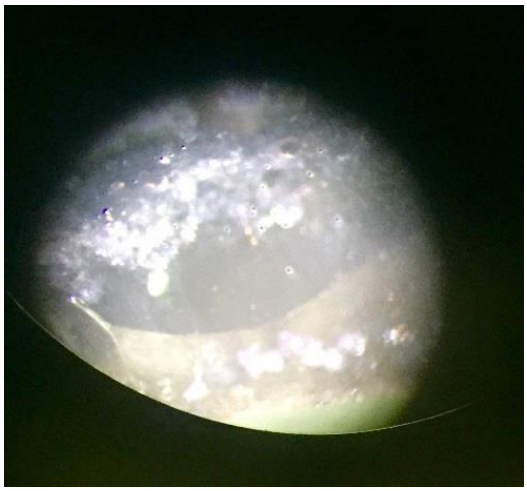

Figure 4- The glassy phase of sample A under the optical microscope (Nikon SMZ-2T)

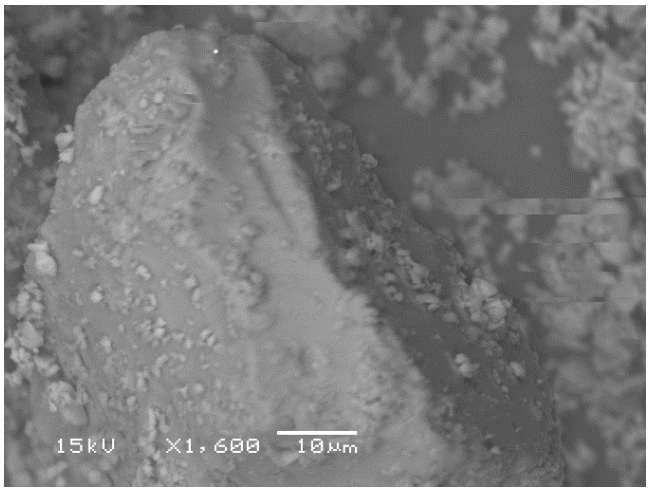

Figure 5- The size of powder after grinding according to the SEM imaging

3.2. Analytical Techniques

In this research a variety of instruments were used for examining the thermal properties of the BFS. They included Hot Stage Scanning Electron Microscope (HS-SEM), Energy Dispersive Spectroscopy (EDS), Computer Aided Thermal Analysis (CATA), Thermogravimetric Analysis (TGA), Fourier Transform Infrared (FTIR) Spectroscopy, and SimaPro LCA.

3.2.1. Hot Stage Secondary Electron Microscopy (HS-SEM)

The SEM used in this study was a JEOL JXA-840 Scanning Microanalyzer, while the hot stage furnace was custom built before the commencement of this work. Figure 6 shows the furnace designed for the Hot Stage SEM experiments.

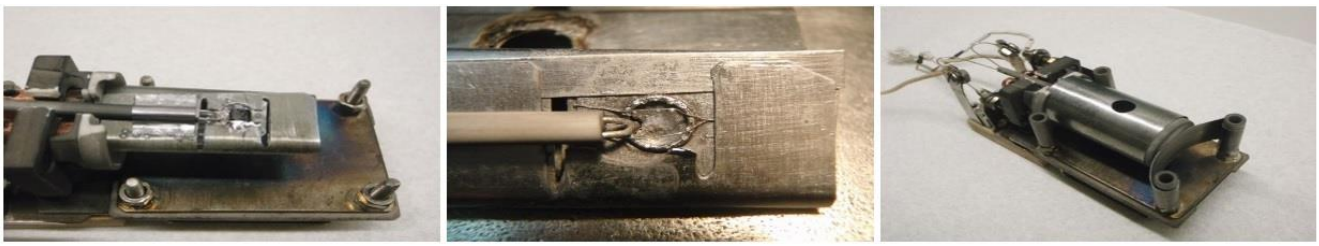

(a) (b) (c)

Figure 6- The mini furnace, devised in the Macquarie University lab used for heating samples inside the microscope chamber; (a) the mini furnace; (b) thermocouples were welded to the molybdenum substrate; (c) molybdenum screening for avoiding heat radiation

In this instrument, two types of signals are used for characterizing the microstructure of the sample. The first is Secondary Electrons (SE) used for morphology and topography of the sample, while the second is Backscattered Electrons (BSE) used for recognizing the different chemical fractions of the sample. SE has little energy, and it is necessary to amplify the energy by the Photon Multiplier Tube (PMT). There is a need to transfer the electrons of SE to photons before amplification with the PMT. The scintillator, located between SE and PMT, is a device used for this purpose. The scintillator is made of glass or plastic, and is not conductive.

HS-SEM is used to recognize the structure of minerals and the changes in this structure during the heat-treatment (Shen et al. 2015). Hot stage in SEM prepares information about the reactivity, phase changes, and crystallization of samples at different temperature (Podor et al. 2012). In this instrument, each sample was heated up to 1500ºC inside the microscope chamber, and the whole process was recorded by the

camera to monitor the morphological changes of the sample during the heating with high magnification (from x12 to x10.000 for slow scanning and x5000 for TV filming) and depth of focus.

Custom built software was used for controlling, recording the temperature and observing the heating process. This software increases the temperature of the sample inside the furnace with the change of current (Power = Voltage × Current). The software also recorded the temperature of two R-type thermocouples, made of Platinum and Platinum/13%Rhodium.Platinum wires.

The substrate is another important factor in this experiment. It is essential to select a substrate that does not have any reaction or interaction with the sample. Moreover, the substrate should have a melting point higher than the sample. The most common substrates are platinum, molybdenum, rhodium and zirconium. To eliminate the possibility that the substrate in a high-temperature experiment could interact with the sample and change its chemical properties, stabilization of the substrate is required. Because the iron content of the studied sample was very small, molybdenum was selected as a substrate for this study. For high iron content slags, platinum substrates may be recommended. In this experiment, two R-type thermocouples were welded to the Mo substrate for controlling the heating and monitoring temperature.

Working distance, which is the distance between the sample and the final lens and typically set to 12 mm, was increased to 25 mm in this study, because of the physical dimensions of the furnace used inside the microscope.

The visual and infrared light, produced from the hot stage, blinds the scintillator. To solve this issue, the scintillator was modified by placing a metal on it, so the visual and infrared light was reflected, and the electrons attracted. Moreover, the heat radiation and electron radiation of the heating process should be managed as well. To reduce the heat radiation, sheltering and screening were applied, and the furnace was sheltered by alumina plate, and screened by a molybdenum strip. For preventing electron radiation, a positive potential was applied to the sample, so electrons are attracted by the positive source. Reflective foil around the furnace and inside the chamber was used to improve the image of the sample during the heating process and to reduce the noise in the images.

The hot stage SEM was used to heat the samples inside the microscope chamber up to their melting point, and the video of the melting process was recorded with a CCD camera. The temperature of the hot stage was manually controlled through a Zero Up (ZUP) 20-10 power supply manufactured by TDK Lambda. The software was developed on the base of LabView Dataloging system (National Instruments™). The

temperature of the hot stage was added by changing the current three times in the ramp from current 5.0A to 7.0A during 300 seconds, and then from 7.0A to 8.0A during 300 seconds, then from 8.0A to 8.6A during 300 seconds. Every step of ramping is for obtaining a better condition for sample melting observations. This particular unit had a variable output capacity of DC 0-10A or 0-20V for up to 200 Watts. The appropriate voltage for the tungsten filament (heater) was rated nominally to 12V for 100W. The sample was then cooled down, and the formation of crystals that appeared on the molten surface during cooling was also recorded. Gold wire was used beside the sample in this stage to calibrate the temperature.

3.2.2. Energy Dispersive Spectroscopy (EDS)

Energy Dispersive Spectroscopy (EDS) is a technique used for analyzing the chemical content of the sample and is used as an attachment to the SEM (Ngo 1999, pp. 205). EDS assists in identifying the weight and atomic percentages of minerals that appear before and after the heat-treatment (Shen et al. 2015). It is also used to analyze the topography of the sample. The advantage of this instrument is the high speed of analysis and the ease of data interpretation (Ngo 1999, pp. 205). In this work EDS was used to study the sample's composition before and after the heating process. EDS was used for obtaining the different ratios of chemical content, such as Ca/Si, which shows the basicity of the sample. This technique is limited to detecting the concentration of elements which are in the order of 0.1% of sample volume. EDS also assisted identification of the chemical composition of the crystals that appeared first in the cooling process.

In EDS, it is important to have a standard sample for calibration with chemical composition, crystalline structure, smooth surface and phase that is close to the sample that is going to be assessed (Rumyantsev et al. 2010). In this experiment, hematite (Fe_2O_3) was used as a calibration for the BFS.

The BFS is not conductive, so electrons aggregate at the surface of the sample and cause a charge effect to discharge the electrons from the surface, like a flash. The charge effect of the sample causes difficulties monitoring the sample, because every few seconds the discharge occurred. To avoid the charge effect, high pressure inside the chamber of the microscope was used instead of carbon coating. The carbon coating of bulk samples was not used in this experiment as it changed the chemical composition of the sample. When the pressure inside the chamber was 30 Pa instead of high vacuum, ions inside the chamber have a positive signal and could discharge negative electrons at the surface of the sample, causing the

charge effect. In this case, the resolution of the SE image was compromised, but was still sufficient enough to conduct the EDS analysis.

In analysing the EDS results, the mass of some elements was omitted, such as carbon because it came from the carbon tape used to stick the sample to the specimen, or other trace elements with a tiny mass in comparison to the total sample (100% mass).

The EDS used was with the JEOL6480LA SEM. In this experiment, the pressure used inside the microscope chamber was 30 Pa, the accelerating voltage was 15 kV, the energy range was between 0-20 keV, and the working distance was 10±2 mm.

3.2.3. Trace Element Analysis

For identification of trace elements, the sample was sent to the National Measurement Institute. The Method they used was a metal analysis performed by inductively coupled plasma mass spectrometry (ICP-MS) and inductively coupled plasma atomic emission spectrometry (ICP-AES). The samples were digested with HNO_3-HCl at 95-100°C for two hours. Then the trace element concentration was measured by ICP-MS and ICP-AES. One control sample and one blank were used in this experiment.

3.2.4. Computer Aided Thermal Analysis (CATA)

The CATA analysis technique was used for calculating the specific heat of the sample. Figure 7 shows the schematic diagram of a thermal analysis instrument in cross section (Strezov 2006). The sample was loaded in a silica glass tube and surrounded by the graphite cylinder. The graphite heating element supplied the heat at the heating rate of 10°C/min. The sample was kept under the inert gas of argon, at 5 ml/min, and the sample was heated to the maximum temperature when the graphite reached 1200°C. In this technique, three thermocouples were used for monitoring the temperature of the graphite as a control, surface of the sample and centre of the sample. Surface and centre temperature delay occurs in heating and cooling due to heat resistance. The specific heat was calculated by the inverse numerical technique using the measured temperatures (Strezov 2006). When the specific heat shows an increase in value, it means that the sample has an endothermic heat effect (Strezov 2006). However, in the exothermic reaction, the specific heat decreases (Strezov 2006).

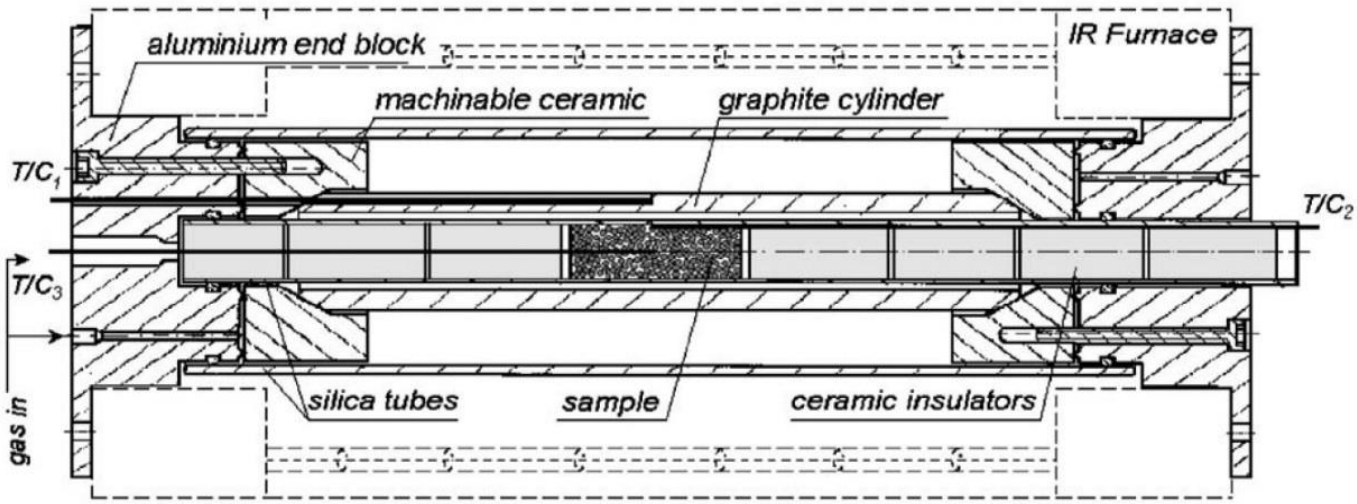

Figure 7- A cross section of the thermal analysis instrument used (Strezov 2006).

3.2.5. Thermogravimetric Analysis (TGA)

Thermogravimetric analysis is a technique that assists in demonstrating the thermal degradation of the sample. TGA investigates the changes in the mass of a sample as a function of temperature or time. In this experiment, approximately 70 mg of sample was placed in an alumina crucible and subjected to TGA analysis in a Mettler Toledo thermogravimetric analyser (TGA/DSC 1 STARe system). Nitrogen gas was used to purge the sample at the rate of 20 ml/min and the sample was heated up to 1000°C at the rate of 10°C/min. The initial weight of the sample was measured in a Mettler Toledo (XS105 DualRange) before starting the experiment. A blank sample was used for calibration of the buoyancy effect of the TGA.

3.2.6. Fourier Transform Infrared (FTIR) Spectroscopy

FTIR spectroscopy is a technique that provides a fingerprint for identifying specific spectra by comparing the spectrum of a new unknown sample with the spectrum of a sample that has been identified and analysed before (Coates 2000). FTIR assists in distinguishing types of samples regarding differing structures, composition and changes in structure resulting from chemical modification (Madejova 2003). The unit of measurement is wavenumber (cm^{-1}) and the average wavenumber recorded is between 4000 cm^{-1} and 400 cm^{-1} (Coates 2000). In this study, FTIR was used to investigate the changes of sample spectra when the sample was heated up to different temperatures (25, 600, 820, 1010, and 1200°C). The sample was initially heated to the temperatures specified in a CATA at a heating rate of 10°C/min under the inert gas argon at 5 ml/min. The sample was cooled down and then subjected to FTIR analysis at a Nicolet 6700 FTIR spectrometer through total 32 scans with a resolution of 4 cm^{-1}.

3.2.7. SimaPro

SimaPro is a technique which assists in analysing and monitoring the sustainability of decisions to be made by the industry. This software supports to measure and improve our products in the life cycle (PRe Sustainability 2013). The software assists with obtaining the data about the sustainable development of each industry and assesses the life cycle, the carbon and water footprint and other environmental aspects (PRe Sustainability 2013). The method helps to compare alternative actions in each industry in a variety of comparisons, such as climate change and ozone depletion in general, or the CO_2 and methane emissions. In this research, SimaPro software was used to compare the effect of slag replacement with Portland cement in the concrete industry. The purpose was to investigate the environmental and commercial benefits of substituting the slag for Portland cement in the concrete industry. The SimaPro LCA ecoinvent version 3.2 software was used in this study.

4. Results and Discussions

4.1. Hot Stage Scanning Electron Microscope

Each of the three samples was melted separately inside the SEM, twice, to investigate the melting point and the crystals that appeared initially in the re-solidification process. Gold wire was used to calibrate the temperature. The melting point of Au is 1064°C, and the melting temperature of Au was evident in the film, which was used to calibrate the temperature and determine the melting point of the samples. According to the thermocouple temperature and time data which came from the custom-built software, the temperature/time differentiation was calculated. The time in the horizontal express the evolution time of the test. Temperature/time differentiation is the temperature in second one and temperature in second two and this is the reason for fluctuation. This curve shows the fluctuation of sample during the time when we start to heat up the sample. The drop in the temperature/time curves shows the melting behaviour and the slope are changed due to the melting behaviour. Moreover, the temperature/time differentiation and film of the melting process were compared to investigate the melting point of each sample in the first and second melting process. It is apparent that the melting of the sample caused the collapse in the diagram of temperature/time differentiation for each sample. In the following figures (Figures 8 to 13), the melting point of each sample was demonstrated by the temperature/time differentiation (by circle around the melting behaviour) and images extracted from the film of the heating process.

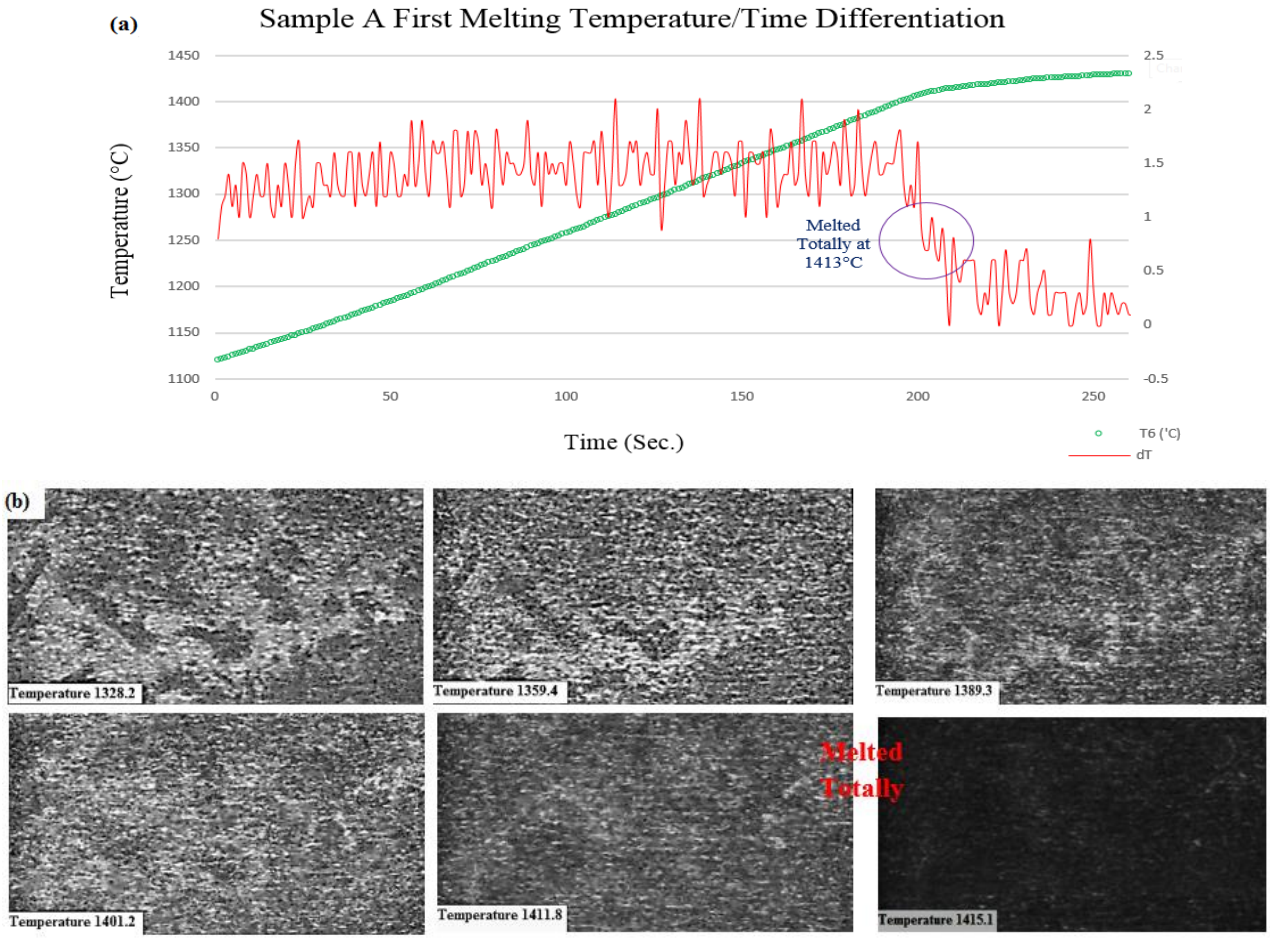

Figure 8- First melting behaviour of sample A; (a) temperature/time differentiation shows the melting point is 1413°C; (b) the images extracted from the film indicate that the sample melted entirely at 1415°C, the sample is completely melted in 200 seconds.

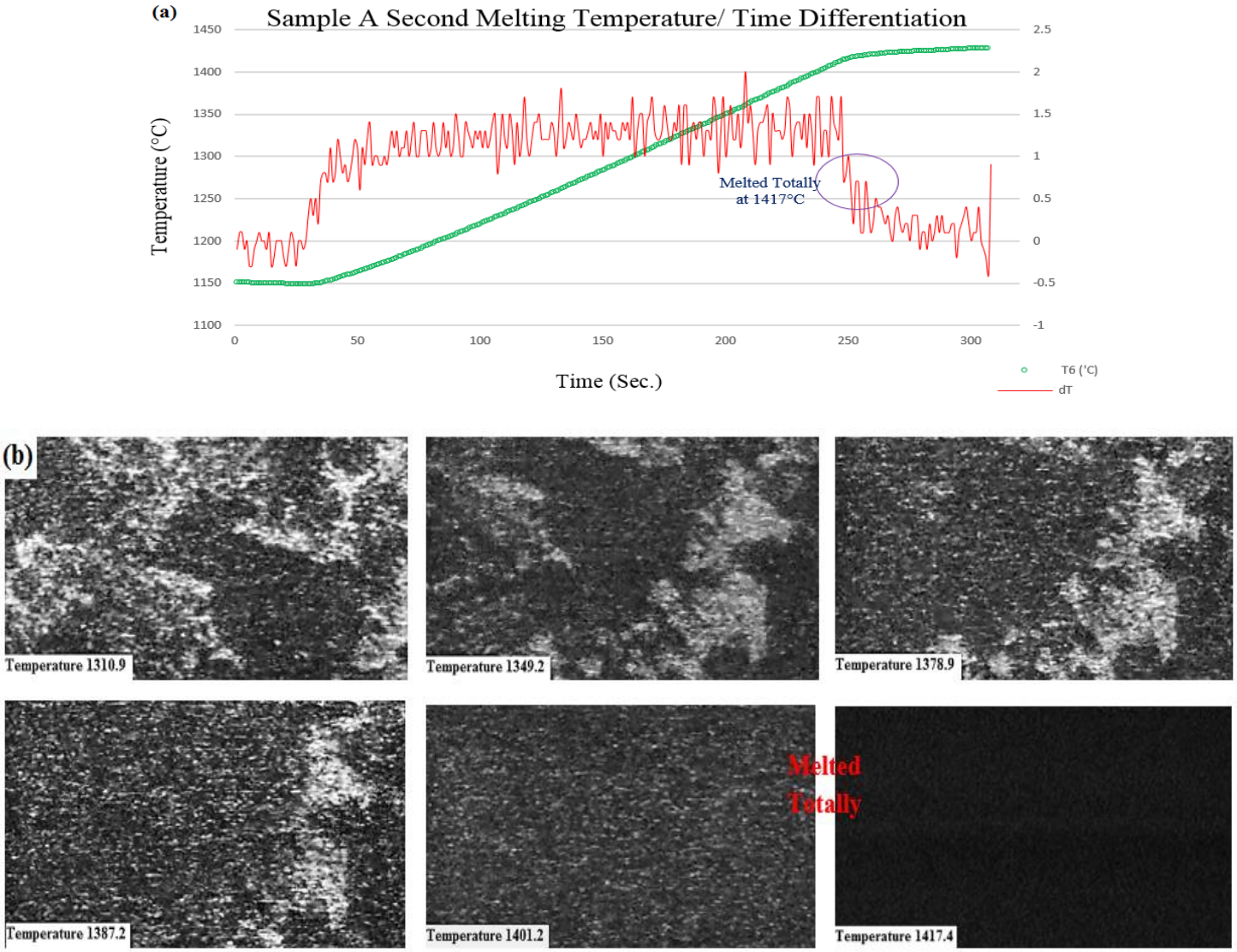

Figure 9- Second melting behaviour of sample A; (a) the chart of temperature/time differentiation shows the sample A is melted for the second time at 1417°C; (b) the film images confirmed that the melting point of sample is at 1417°C, the sample is completely melted in 250 seconds.

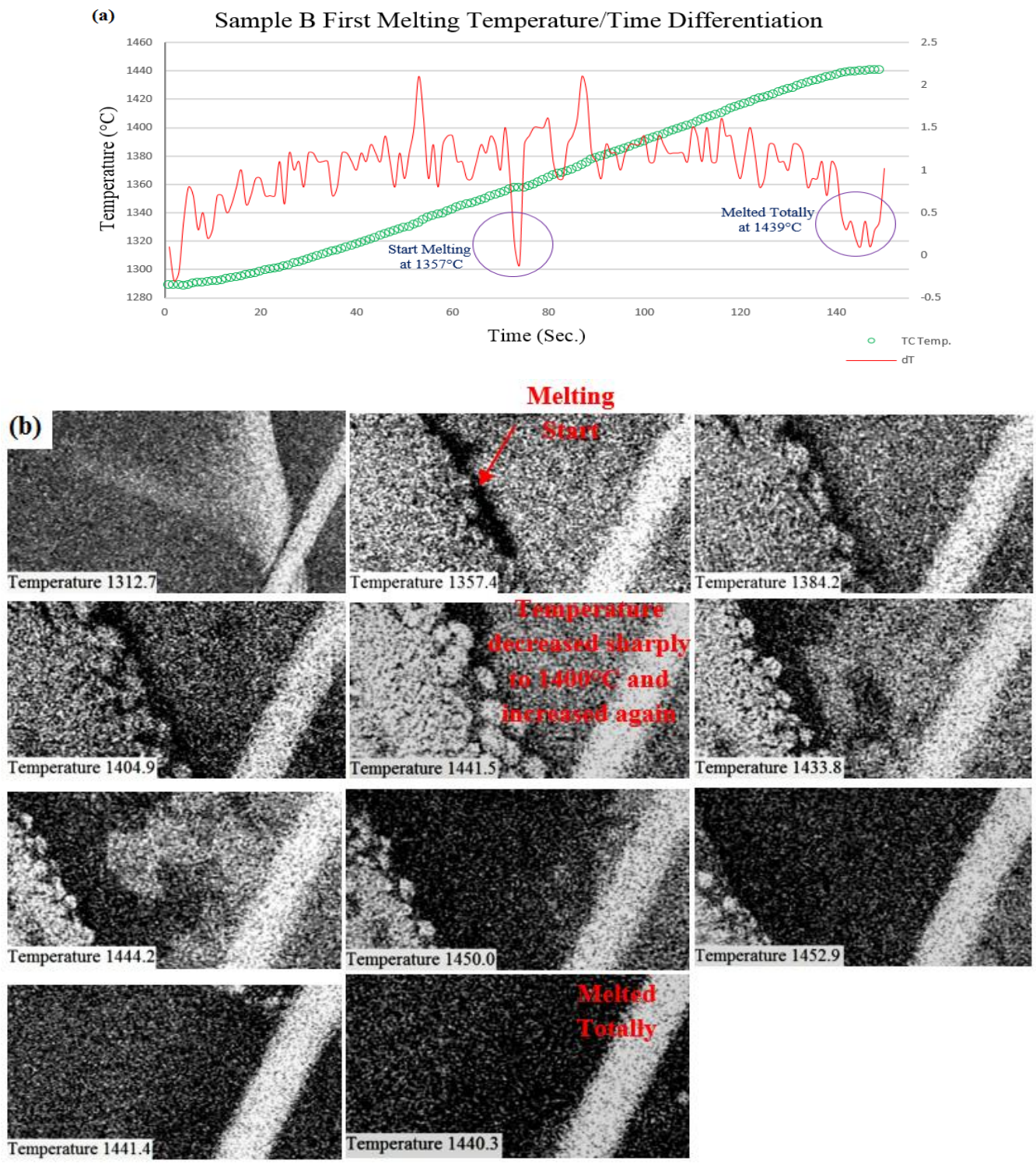

Figure 10- First melting behaviour of sample B; (a) the melting started at 1357°C and sample melted completely at 1439°C; (b) the film images that confirmed those behaviour and melting point of sample, the sample is completely melted in 140 seconds.

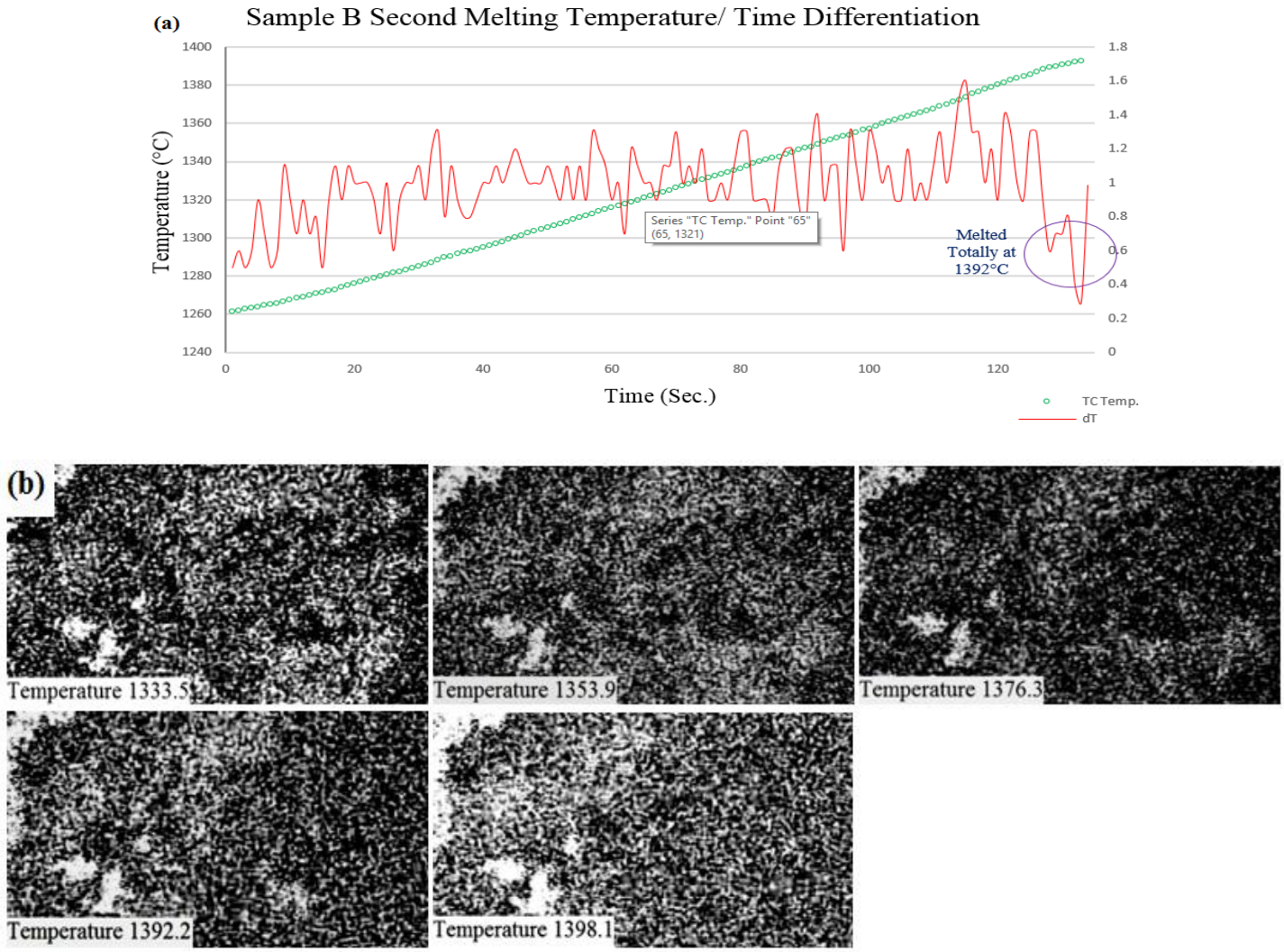

Figure 11- Second melting behaviour of sample B; (a) according to the temperature/time differentiation the melting point of sample in a repeat test was 1392°C; (b) the images almost confirmed this melting temperature, the sample is completely melted in 130 seconds.

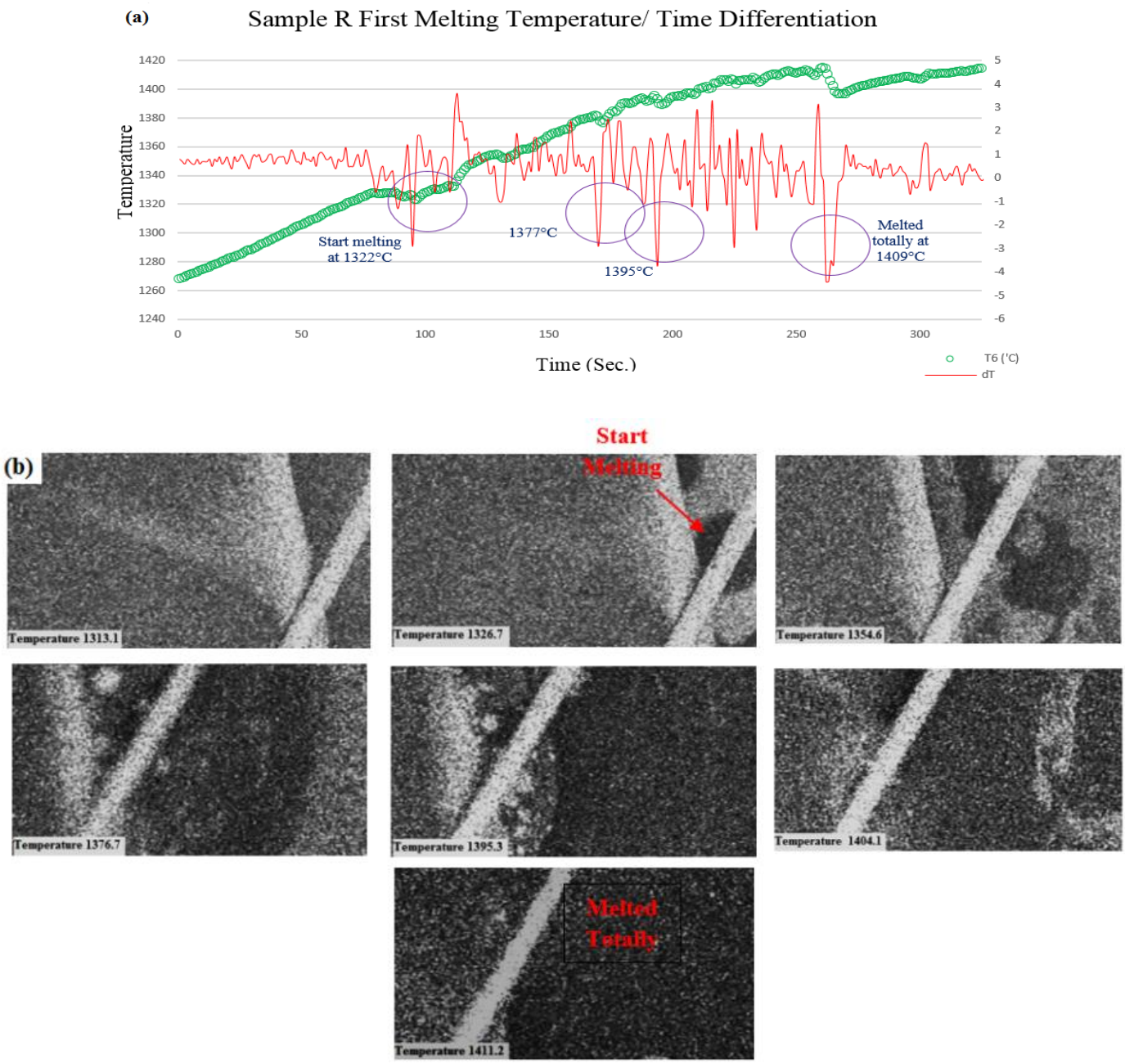

Figure 12- First melting behaviour of sample R; (a) sample started melting at 1322 °C and was melted entirely at 1409°C; (b) the images confirmed those temperatures at 1377 and 1395°C, with temperature/time chart collapse because the surface of the sample was melted, the sample is completely melted in 260 seconds.

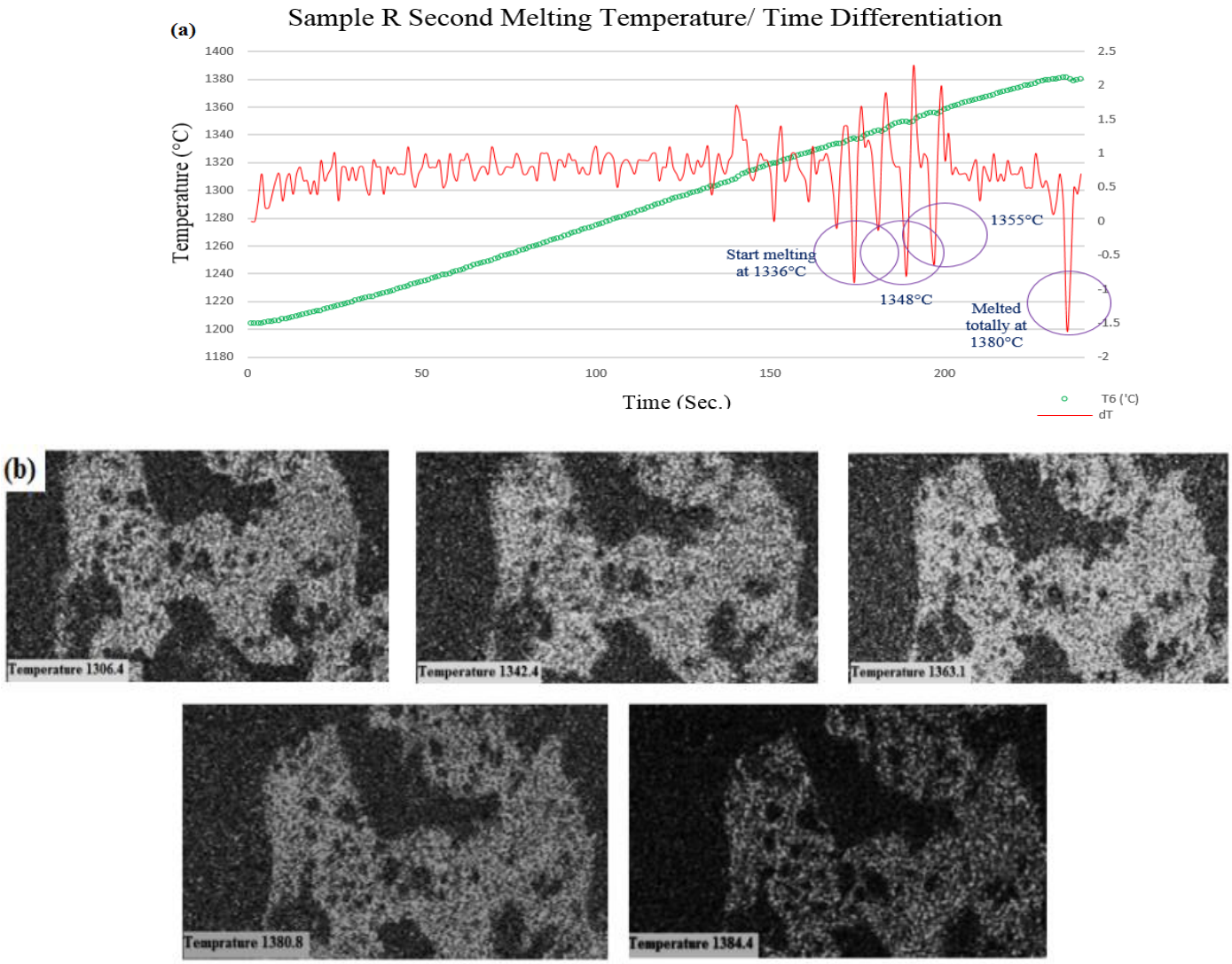

Figure 13- Second melting behaviour of sample R; (a) sample start melting at 1336°C and melted entirely at 1380°C, some melting behaviour is observable due to the surface of the sample and its different composition; (b) the image was not clear enough to investigate the behaviour of melting. It should be noted that, dark area is the melted sample, the sample is completely melted in 290 seconds.

According to the above data (summarized in Table 2) the melting point of each sample is different because of the different chemical compositions. The first melting point of each sample is higher than the second melting point and the reason might be the evaporation that occurred during the first melting and that changed the chemical content of sample. The correlation between basicity (CaO/SiO_2) of each sample with their melting point suggested that higher basicity is associated with greater melting point of the sample. Sample R, which had the lowest basicity (according to the chemical composition), had a lower melting point in comparison with the other two samples. Sample B, with the highest basicity, had the highest melting point. Also, in the repeat heating it was observed that the second melting point is

lower than the first one. The reason of this could be the evaporation that might occur during the first melting.

The sample R had multiple melting point according to the Figure 12 and 13. The reason might be the size of the sample in the HS-SEM test is bigger than sample A and B. When the size of sample is bigger, the surface of sample is melted earlier compared to the deeper part of the sample. The surface that is melted causes the fluctuation in the temperature/time differentiation curve before complete melting of the sample. In the film that is taken from this behaviour, the movement of melted sample is obvious around the bulk sample that is not totally melted.

Table 2- Melting point of samples in first and second melting

Melting Point	First Melting	Second Melting	Basicity (CaO/SiO_2)
Sample A	1415°C	1400°C	1.12
Sample B	1440°C	1398°C	1.22
Sample R	1411°C	1385°C	1.09

The highest melting point was from sample B, which melted at 1440°C, and the lowest melting point was allotted to sample R, which melted at 1409°C. Sample R has the lowest basicity, and the amounts of Al_2O_3 and MgO are higher than the two other samples. On the other hand, the basicity of sample B is the highest among the three samples. These results demonstrate the effect of basicity, which is the amount of CaO/SiO_2, and further suggest that adding the amounts of Al_2O_3 and MgO to the system will affect the melting point and viscosity of slag.

4.2. Energy Dispersive Spectroscopy

The chemical composition of samples was examined by the external laboratory and was also observed by EDS in three stages: bulk, powder and the sample after melting. The results are summarised in Table 4. As can be observed in Table 3, the amount of MgO after the melting and crystallisation process reduced sharply. This indicates that the crystals eject the MgO when re-building their structure. On the other hand, the amount of SiO_2 is increased after melting and crystallisation processes, so the crystals absorb the SiO_2 from their surroundings to build their shape. Furthermore, in Sample B, the amount of Al_2O_3 was reduced after the melting and crystallisation.

Table 3- The chemical composition of samples in bulk and powder types in compare with the external laboratory analysis

Slag		TFe	SiO_2	CaO	MgO	Al_2O_3	MnO	TiO_2	Basicity
Sample A	External	0.43	35.93	40.41	8.38	13.54	0.26	0.5	1.12
	Bulk	0.39	34.222	41.057	9.826	13.746	0.288	0.467	
	Powder	0.32	31.641	43.776	9.263	14.24	0.227	0.531	
	Melted	0.998	39.246	40.544	3.449	14.657	0.194	0.906	1.033
Sample B	External	0.35	33.31	40.94	8.46	14.99	0.26	0.57	1.22
	Bulk	0.225	32.883	39.725	10.826	15.576	0.208	0.558	
	Powder	0.204	29.023	43.485	9.421	16.98	0.232	0.654	
	Melted	0.081	46.693	39.832	1.273	10.597	0.08	1.443	0.853
Sample R	External	0.39	30.78	33.83	13.34	19.01	0.84	0.97	1.09
	Bulk	0.316	29.21	32.713	16.28	19.751	1.006	0.723	
	Powder	0.136	28.71	34.426	15.515	19.051	0.99	1.173	
	Melted	0.098	42.837	35.475	1.093	19.146	0.098	1.25	0.828

When comparing the chemical composition of each sample between the external lab and the sample after melting, it is evident that the content of MgO is reduced sharply in all samples. Additionally, the content of SiO_2 is enhanced as well. Only sample B shows a decrease in the content of Al_2O_3 from 16% to 10.6%. Moreover, when basicity was calculated after the melting point, reduction of basicity in sample B is most significant in comparison with the other samples, and reduced from 1.22 to 0.853. After melting, the basicity of both sample B and R became less than 1 while sample A still had a basicity of above 1.

Each sample after the melting and cooling process has some similarities in their crystalline phase that can be distinguished by EDS. In this step, the main, similar crystallization phases of each sample were discovered. Then, the chemical composition of the top of the crystals and immediately around the crystals was measured. The chemical composition of different crystals and phases is demonstrated in Figures 14 to 16.

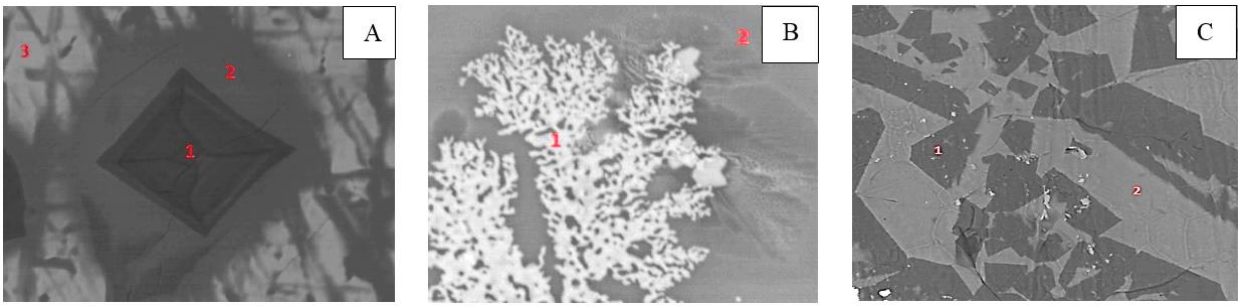

Sample A		TFe	SiO_2	CaO	MgO	Al_2O_3	MnO	TiO_2
	No. 1	0.202	37.796	42.248	4.372	14.89	0.072	0.416
A	No. 2	0	44.8	42.01	1.796	10.04	0.04	1.31
	No. 3	0.21	42.176	41.453	2.535	12.075	0.126	1.426
B	No. 1	0.965	38.145	38.328	3.328	17.776	0.236	1.22
	No. 2	0.314	39.948	39.63	3.506	15.744	0.07	0.786
C	No. 1	0.58	36.451	39.992	5.45	16.708	0.350	0.46
	No. 2	0.208	42.465	40.295	2.774	12.245	0.261	1.747

Figure 14- Sample A had three different phases, and each phase chemical composition is listed. Sample A absorb the MgO and Al_2O_3 for building the crystal shape, and the dark area of images have more MgO and Al_2O_3 especially in the image (a) and (b). Also, the SiO_2 was ejected from the top of the crystals.

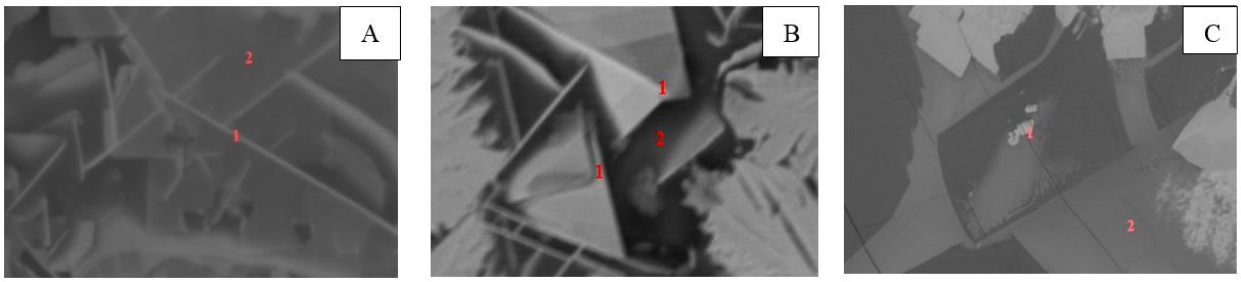

	Sample B	TFe	SiO_2	CaO	MgO	Al_2O_3	MnO	TiO_2
A	No. 1	0.068	48.210	39.255	1.53	8.965	0.027	1.945
	No. 2	0.043	50.273	39.923	0.419	8.013	0.098	1.23
B	No. 1	0.146	49.436	40.386	0.583	8.413	0.066	0.97
	No. 2	0.072	48.08	40.2	1.465	8.757	0	1.422
C	No. 1	0.078	31.56	39.972	3.674	24.53	0.092	0.094
	No. 2	0.125	44.198	41.452	0.972	11.91	0.066	1.277

Figure 15- Sample B different phases and the chemical composition of crystals. The pyramid and dendrite are two types of crystal phases that were significant in this sample. The pyramid ejected all the MgO to build this shape and in the top of the pyramid there is almost no MgO. On the other part of the sample, the dark area has more MgO in comparison with the bright area. The point is in the dark area of the phase of the image (c) the amount of Al_2O_3 increases sharply.

	Sample B	TFe	SiO_2	CaO	MgO	Al_2O_3	MnO	TiO_2
A	No. 1	0.427	44.91	36.485	0.025	17.2	0.187	0.76
	No. 2	0.023	35.67	35.686	1.203	26.923	0.126	0.366
B	No. 1	0.075	47.158	35.247	0.341	15.187	0.053	1.935
	No. 2	0.01	41.566	31.936	2.133	23.753	0.123	0.473
C	No. 1	0.04	47.159	35.429	0.14	15.428	0.177	1.623
	No. 2	0.042	37.308	34.567	1.411	26.082	0.07	0.518

Figure 16- Sample R phases and chemical composition. In this sample, the pyramidal crystals ejected the MgO and Al_2O_3 as well, and the area surrounding the pyramid crystals has a high amount of Al_2O_3, while the dark area has more MgO and Al_2O_3 in comparison with the brighter area.

The reason for the decrease in the amounts of MgO could be the ejection of this content from the crystalline phase for building their structure. This applies especially for the pyramid crystals, which occur in samples B and R, which have the lowest MgO and Al_2O_3 in comparison to their surroundings. However, the crystalline phase of sample A with crystals and lake around the crystals shows opposing amounts of MgO and Al_2O_3. These types of crystals absorb the MgO and Al_2O_3 to enhance their structure and the amount of these two compounds in the lake of crystals is less than the surrounding area. This indicates that the crystals absorbed these compounds from the lake and incorporated them in the crystal build up.

Finally, the chemical content of the samples in the different phases measured shows that the samples are in melilite saturation. This is apparent in Figure 17 which is a ternary diagram of BFS after 1500°C. When the sample composition is compared with this diagram the type of saturation can be recognised. Furthermore, when the phases of the samples, which were melted and cooled slowly, are compared to the Slag Atlas, it is evident that the samples investigated in this work are melilite.

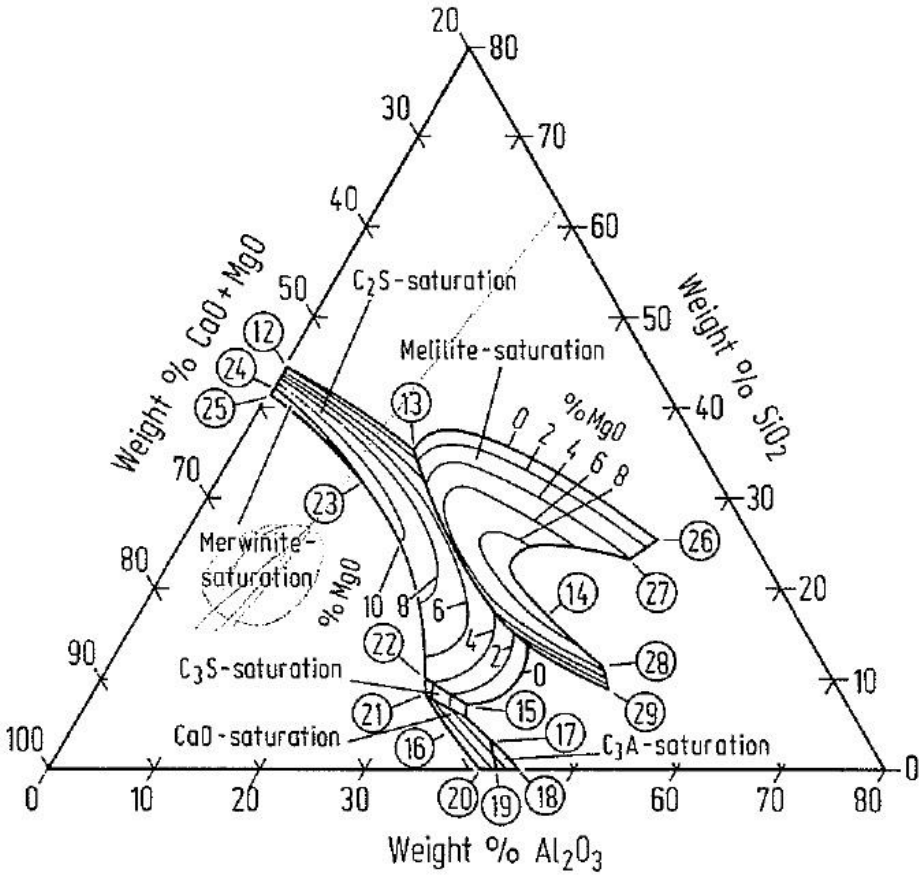

Figure 17- the BFS composition at 1500°C (Eisenhuttenleute 1995)

4.3. Trace Elements Analysis

The trace elements of the samples are shown in Table 4. The amounts of potassium, sodium and sulphur are high in comparison with other trace elements. This content may help the recycling project of BFS as compost or other valuable material. BFS has high capacity of phosphorous sorption (Johansson & Gustafsson 2000). Thus, it can be used as an alternative filter material for removing phosphorous from wastewater (Johansson & Gustafsson 2000). For removing the phosphorous large amount of calcium and alkaline condition (pH > 9) is required (Johansson & Gustafsson 2000). The phosphorous of slag can also be reused as a fertilizer (Dippenaar 2005). According to Batty and Younger (2004), BFS can be used for water treatment that has been polluted by high concentration of phosphate.

Table 4- The trace elements of each sample

(mg/kg)	Sample A	Sample B	Sample R
Chromium	10	8.4	27
Cobalt	16	13	15
Copper	<0.5	0.55	0.56
Lead	<0.5	<0.5	<0.5
Nickel	<0.5	<0.5	<0.5
Phosphorous	39	86	110
Potassium	3530	3520	3910
Sodium	2050	1970	2550
Strontium	860	930	530
Sulphur	2770	2690	2090
Vanadium	13	20	77
Zink	3.4	9.1	2.2

BFS has a high capacity for phosphorus sorption (Johansson & Gustafsson 2000). Thus, BFS can be used as an alternative to filter material for removing phosphorous from wastewater (Johansson & Gustafsson 2000). For removing the phosphorous large amounts of calcium and alkaline conditions (pH > 9) is required (Johansson & Gustafsson 2000).

4.4. Computer Aided Thermal Analysis

In Figures 18 to 20, the thermal behaviour and the specific heat of each sample are shown. Part (a) of these figures are CATA curves that are used for monitoring purpose, and part (b) are related to the specific heat which is calculated for obtaining endothermic or exothermic behaviour of each sample.

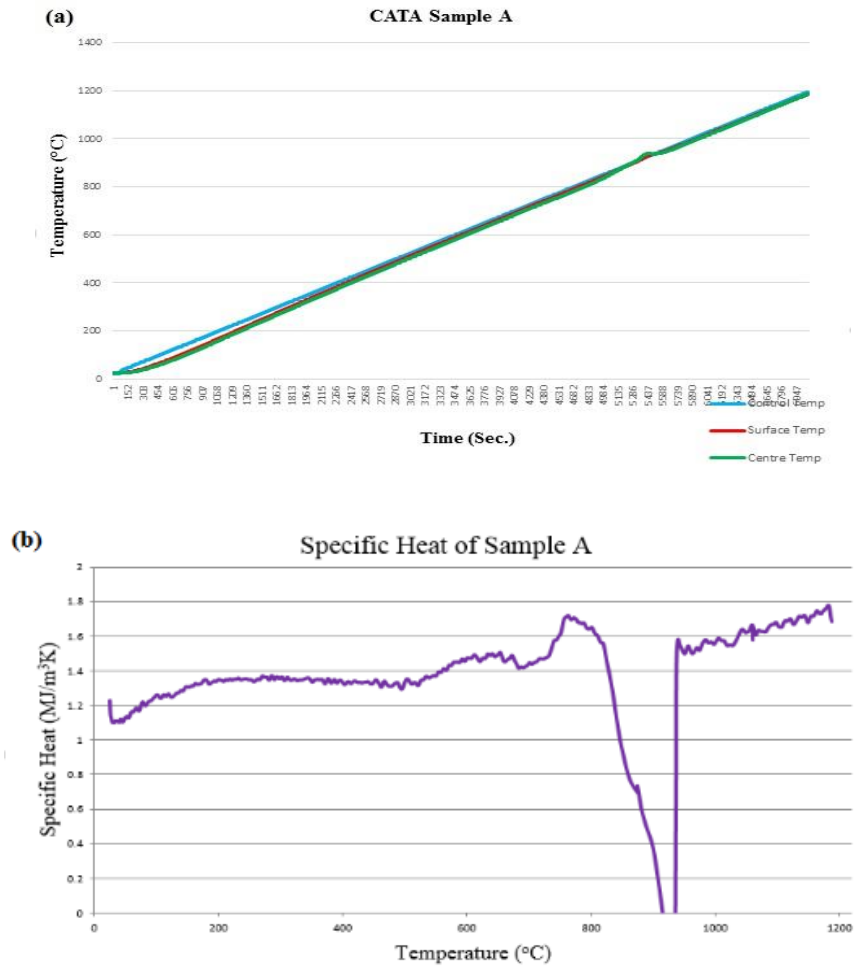

Figure 18- Thermal analysis of sample A, (a) temperatures during heating and (b) apparent specific heat

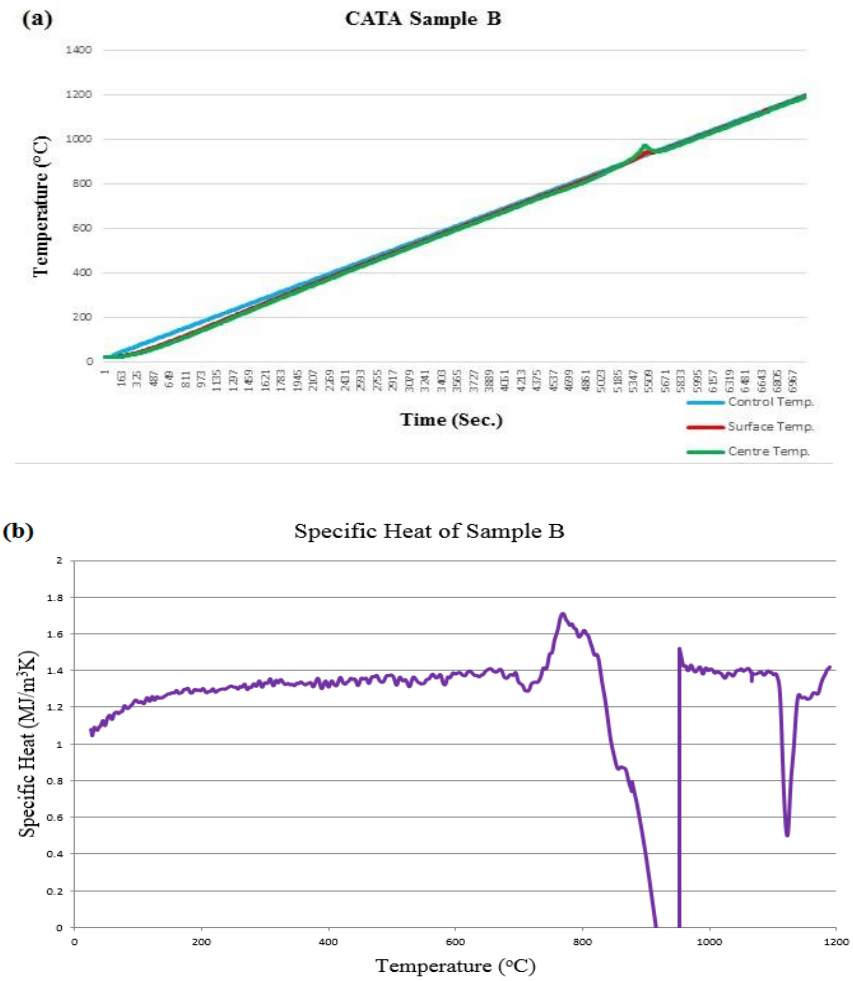

Figure 19- The sample B CATA data shown in (a); and chart (b) demonstrate the specific heat of sample B, and two exothermic behaviour at 827-965°C and 1110-1137°C are evident.

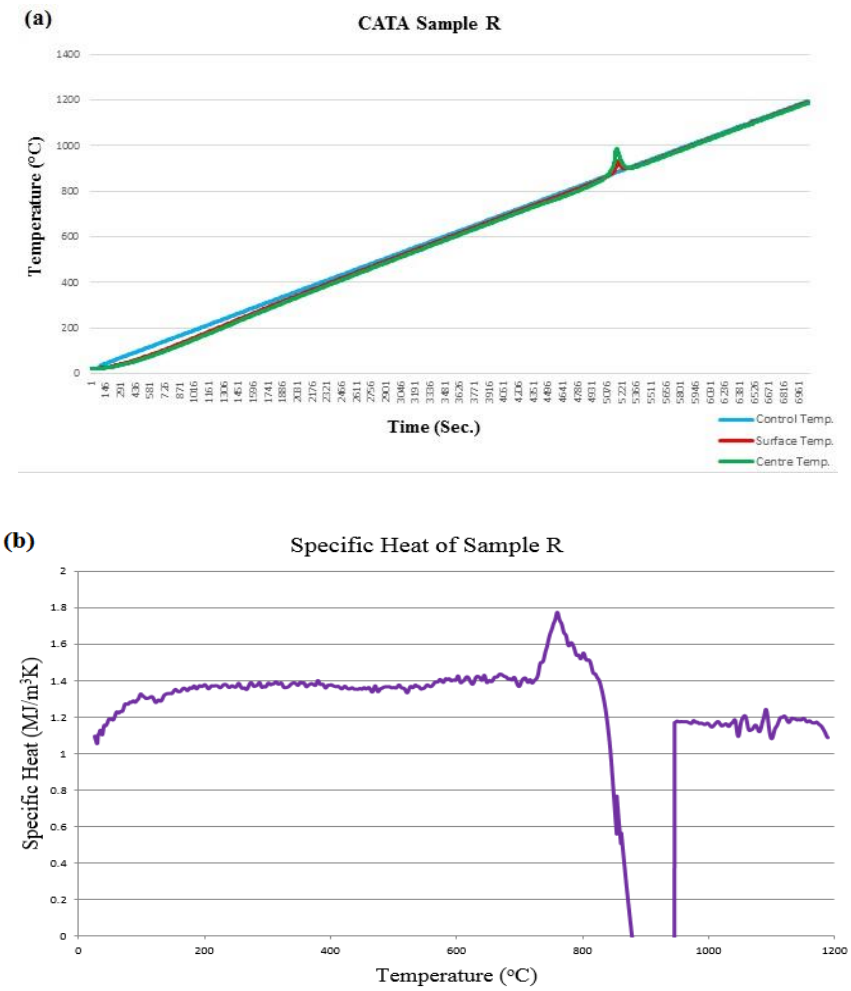

Figure 20- The sample R thermal analysis by CATA (a); and chart (b) display the specific heat and demonstrates exothermic effect between 826-959°C

The results of these experiments show the endothermic and exothermic behaviour of the samples at different temperatures. The endothermic effect starts from 720°C and it continued up to 810°C. This endothermic effect was followed by an exothermic effect in all three samples. The endothermic effect is almost the same in all three samples.

Sample A had one exothermic reaction between 827°C and 937°C. On the other hand, sample B had two exothermic reactions at temperatures of 827°C and 965°C and 1110°C and 1137°C. Finally, sample R had one large exothermic effect between 826 and 959°C and, as it is evident in Figure 20 (a), the interior temperature of sample R increased to 985°C while the control graphite temperature showed 882°C. It means that the temperature of the sample was increased by about 100°C with the exothermic effect and this sharp exothermic reaction occurred in sample R. The exothermic temperature change in sample B and A is smaller than sample R and is about 40°C and 5°C for sample B and A respectively. The

exothermic events of all three samples occur between 828°C and 960°C; however the extent of this effect is stronger in sample R and weaker in sample A. Nevertheless, sample B demonstrated one more exothermic effect between 1110 and 1137°C, which was not as high as the first exothermic reaction.

4.5. Thermogravimetric Analysis

TGA demonstrated the changes in sample weight while it was heated. Figure 21 demonstrate the TGA curves of all three samples and compare them in one graph.

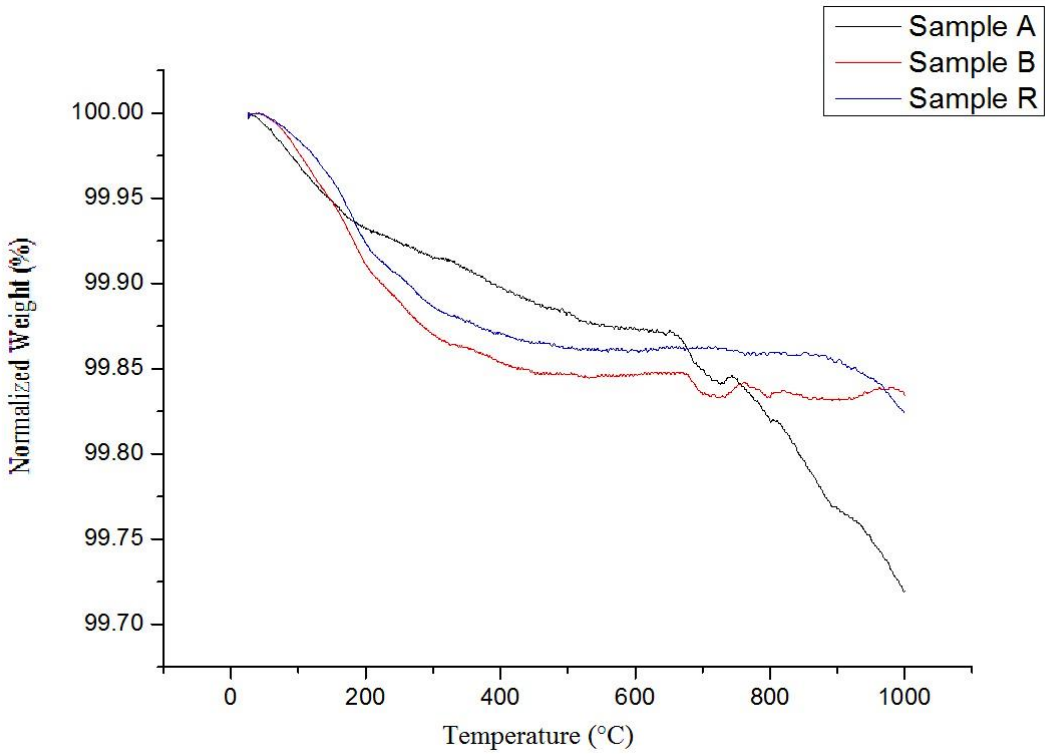

Figure 21- The comparison of weight loss in the three samples.

The TGA of the three samples shows one mass reduction up to 200°C, which is related to the removal of the moisture content of the samples. Sample A and B demonstrated another reduction in weight between 680-755°C, but at this temperature sample R did not show any changes. Sample A after, 755°C, continued to reduce in 0.12 % of its weight up to 1000°C while sample B reduced 0.02 % once more at 800°C. However, Sample R did not show any reduction in weight until 920°C and after this temperature it reduced about 0.02 %.

4.6. Fourier Transfer Infrared Spectroscopy

The FTIR Spectra for BFS for a wavenumber range between 1200 and 400 cm^{-1} for the three samples are shown in Figures 22 to 25. For sample A and R there was no changes at 1010°C in their CATA data; consequently, we did not measure the FTIR for these two samples at 1010°C. The wavenumber regions have a different type of vibration, as determined by Park et al. (2012), such as symmetric stretching bands of $[SiO_4]$-tetrahedra, asymmetric stretching of $[AlO_4]$-tetrahedra and the symmetric Si-O bending vibration. The wavenumber between 1200 and 800 cm^{-1} relates to the $[SiO_4]$-tetrahedra symmetric stretching vibration bands. The Si-O bending vibration associated with the high degree of polymerisation and depth of FTIR transmittance shows that from 600 to 520 cm^{-1} the slag becomes depolymerised. The wavenumber of 400-600 cm^{-1} is related to the Si-O-Si and Si-O-Al connection (Yue et al. 2014). Additionally, 600-800 cm^{-1} is linked to the establishment of Si-O-Al from SiO_4 and AlO_4 tetrahedral (Yue et al. 2014). According to the previous experiments, the increase of SiO_2 causes the growth in the 600-800 cm^{-1} wavenumber region (Yue et al. 2014). The region of 800-1300 cm^{-1} is assigned to the vibration of SiO_4 tetrahedral with a varying number of non-bridging oxygens. In summary, the increase in the SiO_2 content will increase the network rigidity (Yue et al. 2014). According to Memon et al. (2013) there is internal vibration at 963 cm^{-1} and 494 cm^{-1} due to the $[SiO_4]^{4-}$ and $[AlO_5]^{5-}$ tetrahedral. 963 cm^{-1} is related to antisymmetric stretching vibration of Si(Al)-O, and the 494 cm^{-1} is related to the vibration of Si-O-Si (Memon et al. 2013). The weak band, at 711 cm^{-1}, is related to the symmetric stretching vibration of Si-O-Si, and 876 cm^{-1} is related to the asymmetric stretch of the AlO_4^{-1} group (Memon et al. 2013).

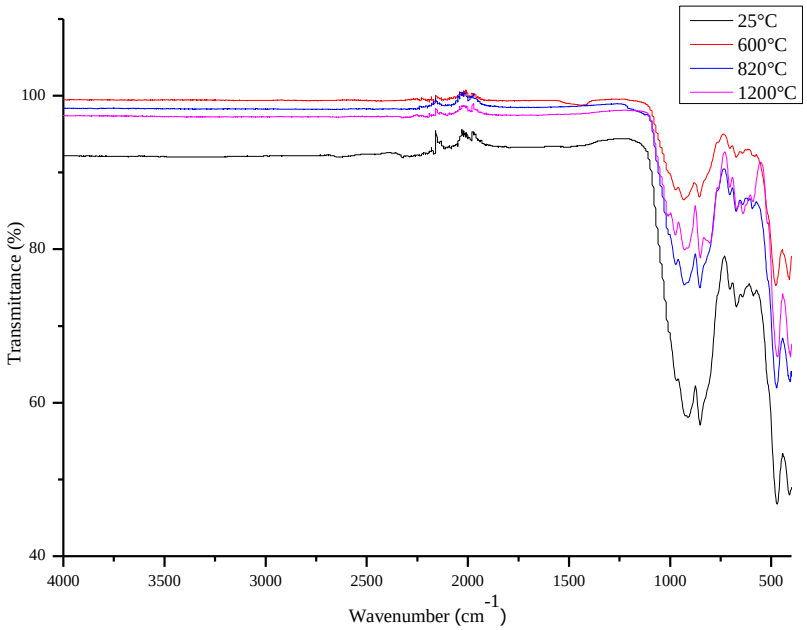

Figure 22- Sample A FTIR spectroscopy

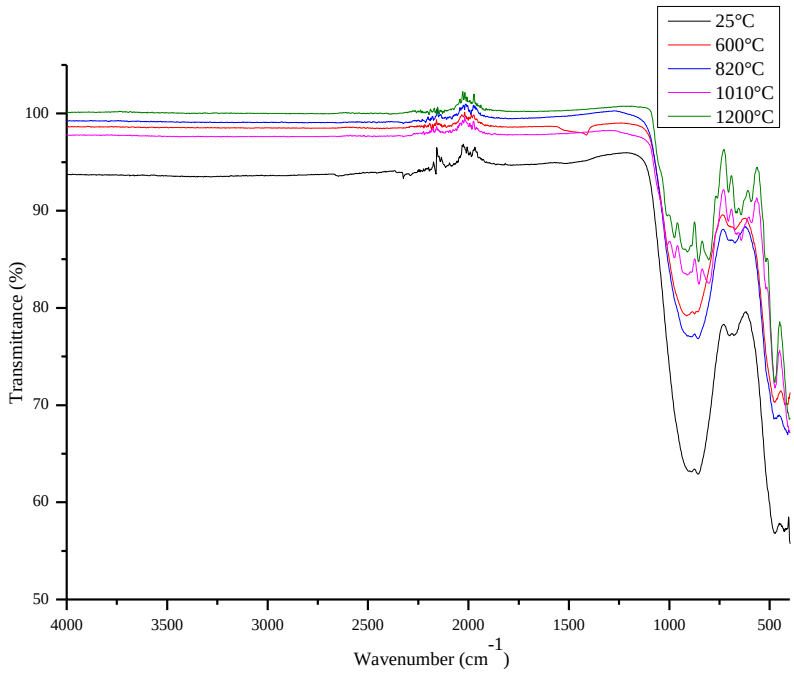

Figure 23- Sample B FTIR spectroscopy in all mentioned temperatures.

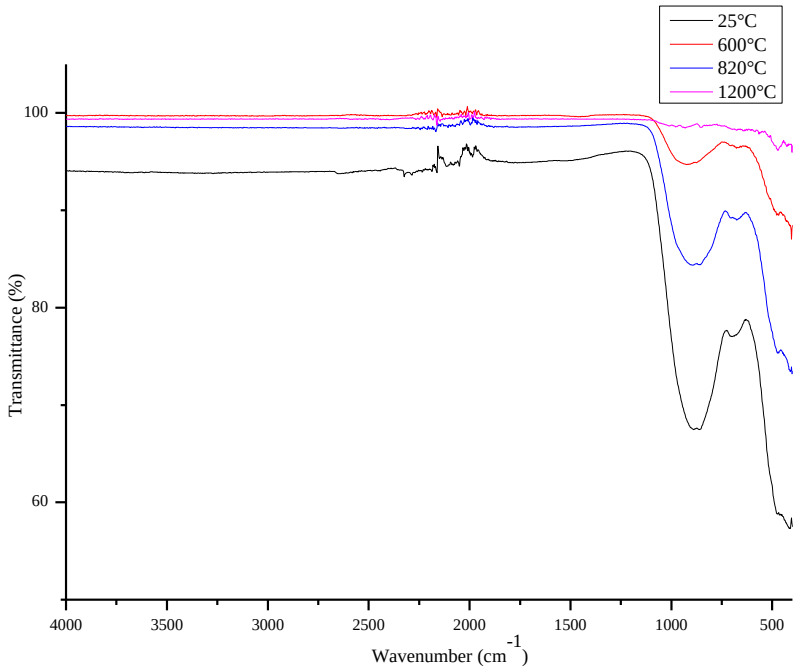

Figure 24- Sample R FTIR spectroscopy, as it is obvious, at 1200°C there is less changes in transmittance.

FTIR Spectroscopy of these three samples shows changes in wavenumber of 916, 687, and 450 cm^{-1}. Moreover, the samples are heated at a different temperature to see the effect of exothermic behaviour and loss of weight on the FTIR spectra. According to the Yue et al. (2014) the 916 cm^{-1} wavenumber is related to the $[SiO_4]$-tetrahedral and 687 cm^{-1} is related to the establishment of Si-O-Al from $[SiO_4]$-tetrahedral, the last wavenumber (450 cm^{-1}) is for Si-O-Si and Si-O-Al connections. When the sample is heated up to 820°C the variation in the transmittance in all three samples is more than the time that the sample was heated up to other temperatures (such as 600, 1010, 1200°C) and this is overlapped by the temperature of the exothermic behaviour of samples. In addition, when samples did not heat (at 25°C) they have the highest change in transmittance in mentioned wavenumbers in comparison to the time that samples were heated to the specific temperature. Sample A has the highest amount of SiO_2 and lowest amount of Al_2O_3 and the changes in transmittance at wavenumbers of 916, 687, and 450 cm^{-1} is more than samples B and R. On the other hand, sample R with lowest amount of SiO_2 and highest amount of Al_2O_3 has the lowest change in transmittance in mentioned wavenumber. Consequently, the increase in the content of SiO_2 will increase the network rigidity in our three samples (Figure 25). In all three samples, the variations of transmittance in the three mentioned wavenumbers are overlapped with the exothermic behaviour of samples.

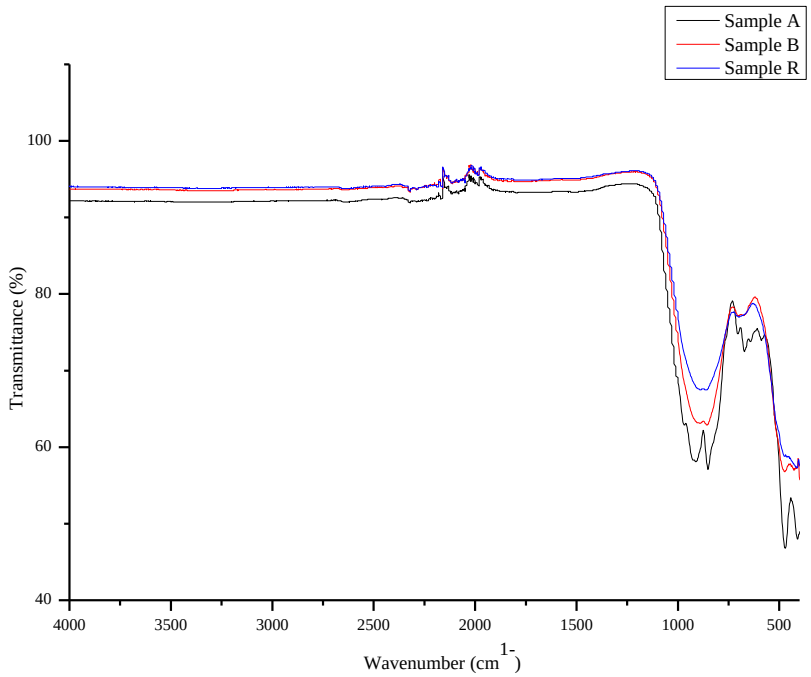

Figure 25- Spectra of all three samples are compered in one diagram to differentiate the effect of different chemical compositions in the spectra of different samples.

This experiment confirmed that the amount of SiO_2 affected the network rigidity. When the amount of SiO_2 decreased from Sample A (with the highest amount of SiO_2 which is about 35.93) to sample R (with the lowest amount of SiO_2 of about 30.78) the network rigidity is enhanced. As the amount of SiO_2 decreased from A to R and the depth of transmittance reduced from A to R in 916, 687, and 450 cm^{-1}, it is suggested that high amounts of SiO_2 cause stronger transmittance in the wavenumbers.

4.7. SimaPro

According to the SimaPro software, when the amount of slag is increased from 0 to 100% in concrete production the general environmental impact will be reduced (Figure 26). For instance, the comparison of BFS replacement from 0% to 100% shows that the climate change, terrestrial acidification, marine eutrophication and other environmental issues will be reduced. Also, considering CO_2 emissions, with slag replacement from 0 to 100%, it is evident that the emission of CO_2 is reduced from ~1 kg CO_2eq to 0.21 kg CO_2eq (Table 5). Additionally, Figure 27 compares the environmental effect of ordinary Portland cement with the condition when the 30% of the concrete is GGBFS. In this research, 30% BFS was

selected as the optimum amount of slag that can be replaced in the concrete industry with Portland cement. When 30% of the Portland cement is replaced with BFS in concrete manufacturing, it still haS environmental effect on different aspects; however, the overall issue will be diminished by this replacement. For instance, the climate change is reduced 24% when 30% of BFS is replaced and, according to Figure 27, the effect of cement industry on global warming is reduced from 87% to 77% by replacing the 30% with BFS.

When the amounts of replacement slag in concrete manufacturing increased from 0% to 100% some environmental indicators decrease significantly, such as metal depletion (condensed from 100% to 0%), fossil depletion (reduced from 100% to 0%), terrestrial ecotoxicity (diminished from 100% to 13%), and climate change (decreased from 100% to 21%). On the other hand, some of the environmental elements are increased by increasing the replacement of slag in concrete industry, such as ozone depletion (from 86% to 100%) and natural land transfer (from 93% to 100%).

Table 5- The exact amount of carbon dioxide emissions when exact amounts of slag are used instead of Portland cement in concrete manufacturing

Amount of slag	***0% Slag***	***10% Slag***	***20% Slag***	***30% Slag***	***50% Slag***	***75% Slag***	***100% Slag***
Kg CO_2eq	0.99	0.91	0.84	0.75	0.6	0.4	0.21

From the SimaPro software results, it is evident that substituting 30% of Portland cement with BFS will reduce the CO_2 emissions. Although it is impossible to remove all Portland cement in concrete manufacturing, the highest possible slag replacement will reduce the environmental footprint of this industry. The large amounts of slag replacement will affect the quality of concrete and reduce the strength of concrete at the early ages. In Table 6, the economic allocation of slag and pig iron are presented (Grant 2015). The SimaPro system helps decision making based on the economical and environmental interest (Chen et al. 2010). In this system, recycling of waste adds no further environmental pollution as these materials are produced already as a part of another industrial activity (Chen et al. 2010). In Table 7 the impact of GHG emissions (kgCO_2-eq) per m^3 are shown and, as evident, the replacement of even 30% with slag will have the effect on the GHG emissions (Grant 2015). When comparing these data with the price of BFS, the economical and environmental benefits of this replacement are apparent.

Table 6- Economic allocation for slag

Product	Mass Produced in kg	Market Price in A$/t	Allocation by Mass Value	Allocation by Economic Value
Pig Iron Content	1.0	503.00	80%	99.682%
Slag Content	0.25	6.41	20%	0.318%

Table 7- Compare the impact of normal concrete and the concrete with 30% slag

Type of Concrete	Unit	20 Mpa	25 Mpa	32 Mpa	40 Mpa	50 Mpa
Ordinary Portland Cement Concrete	$kgCO_2$-eq	318	356	409	493	623
Concrete 30% GGBFS	$kgCO_2$-eq	256	288	329	396	502

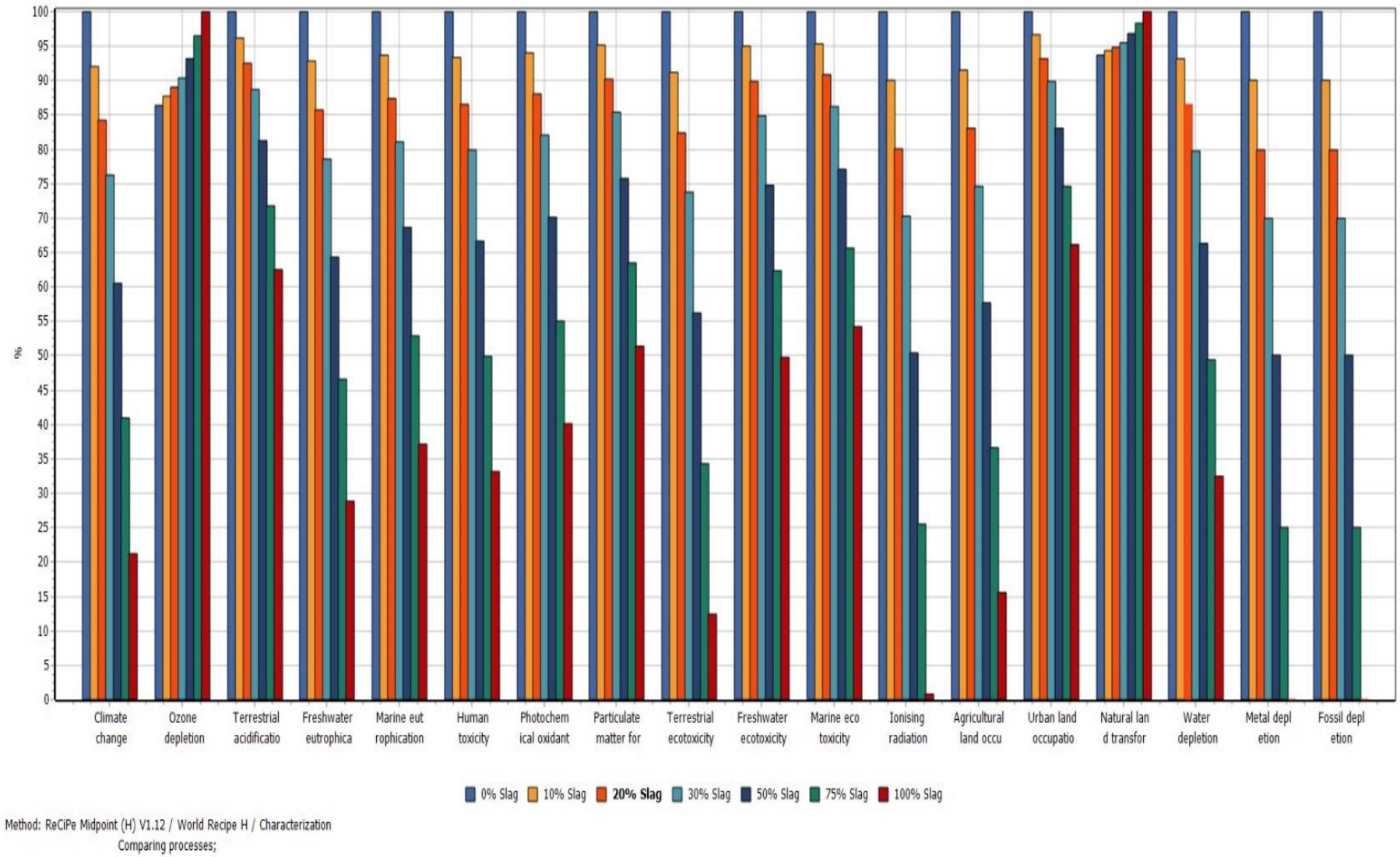

Figure 26- Summary of the environmental effects of slag replacement from 0% to 100% in the concrete industry

(a)

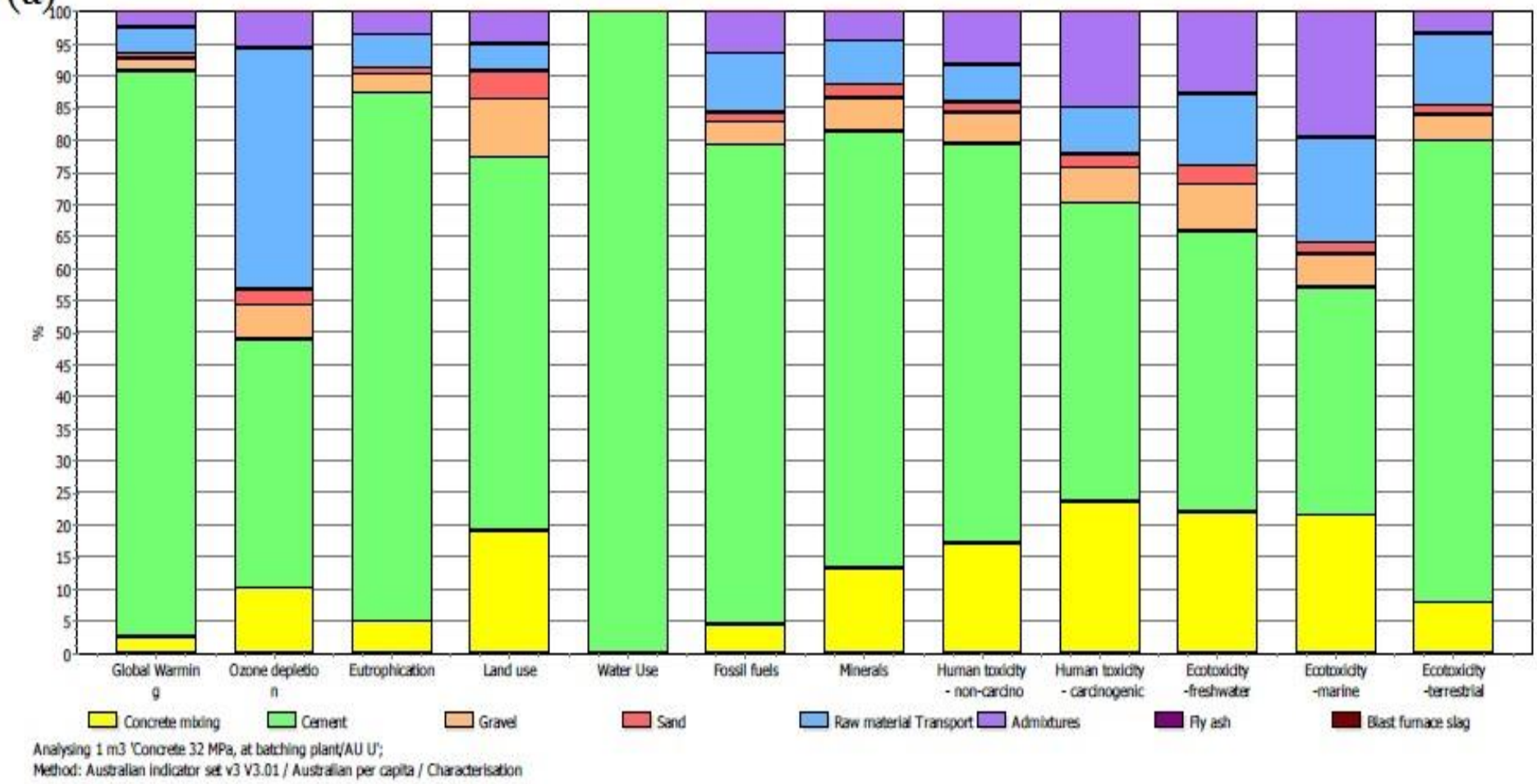

Analysing 1 m3 'Concrete 32 MPa, at batching plant/AU U';
Method: Australian indicator set v3 V3.01 / Australian per capita / Characterisation

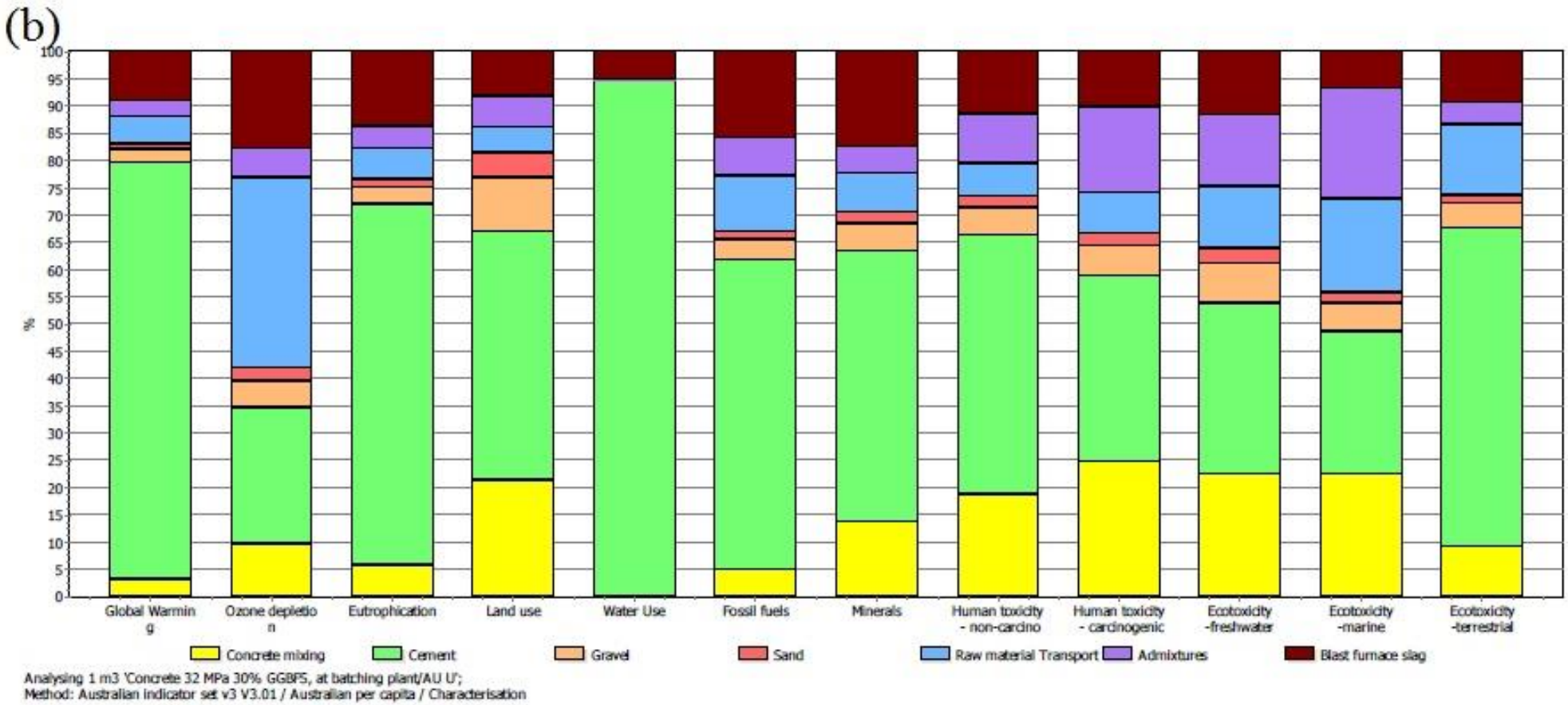

Figure 27- Compare (a) ordinary Portland cement and (b) concrete with 30% GGBFS, the 30% was chosen as an optimum amounts of BFS that can be replaced by Portland cement without changing its strength and hydraulic properties of cement and concrete.

5. Conclusions and Recommendations

Iron is one of the most common metal used worldwide. The amount of iron ore produced in 2014 was 3.22 billions of tonnes and this amount increases every year as the demand increases (Iron Ore & Global market 2015). China with 1.5 billion tonnes is the largest producer of iron ore and the second largest is Australia with 660 million tonnes of iron ore produced each year (Iron Ore & Global market 2015). On the other hand, concrete is another important material for development and it is produce at a rate of about 10 billion tonnes per annum (Meyer 2009). Any improvement in the efficiency of these industries will have the significant effect on the environmental and economical aspects. Recycling the energy in the iron making and recycling the slag, which is a by-product, will have positive global implications, both economically and environmentally.

This study has important outcomes summarised below:

- The basicity has the direct effect on the melting point of the slag as higher basicity increases the melting point. Furthermore, the high amount of Al_2O_3 and MgO might have an effect on the melting points of the BFS, but this needs further investigation.
- The amount of MgO in the crystalline part of the cooled slag is remarkably low in comparison to the initial amounts before the heating and cooling processes. We could conclude that the crystalline phase could not appear in the BFS with high amount of MgO.
- The samples had exothermic behaviour at a temperature range of 828°C and 960°C. When comparing these data with FTIR, it is evident that the amount of SiO_2 had an effect on this behaviour, especially in 916 cm^{-1} wavenumber.
- With replacement of every 10% of Portland cement, the GHG emission is reduced according to the SimaPro analysis. Moreover, other environmental indicators, such as fissile depletion, metal depletion, and terrestrial ecotoxicity, are reduced by this replacement.

These findings suggest potential energy saving by re-directing heat energy in slag to reduce heating energy input when heating pig iron. Further incorporation of slag as cementations products will cut raw material input as well as reduce waste disposal problems and costs. Further advances will occur if the higher value end use of slag is discovered and reduced the industry costs and demands for other raw materials or resources.

Some recommendations are listed below for further work:

- The viscosity of BFS and relationship between viscosity and chemical composition is required which will assist at find the way to reduce the viscosity. The method which reduces the viscosity should be applicable by the industry.
- The heat energy transfer from the BFS to the pig iron while maintaining the value of slag for the end use should be better engineered.
- The BFS characterisation should be further studied to investigate the better recycling options with the optimum economical value.
- Examining the factors that are affected by the replacement of Portland cement with BFS using SimaPro.

6. References

Barati, M, Esfahani, S, Utigard, T, 2011, 'Energy recovery from high temperature slags', *Energy*, vol. 36, pp. 5440-5449.

Batty, L, Younger, P, 2004, 'The use of waste materials in the passive remediation of mine water pollution', *Surveys in Geophysics*, vol. 25, pp. 55–67.

Bisio, G, 1997, 'Energy recovery from molten slag and exploitation of the recovery energy', *Energy*, Vol. 22, No. 5, pp. 501-509.

Brodnax, L, Rochelle, G, 2000, 'Preparation of calcium silicate absorbent from iron blast furnace slag', *Journal of the Air & Waste Management Association*, vol. 50, pp. 1655-1662.

Chen, C, Herbert, G, Bouzidi, Y, Jullienc, A, Ventura, A, 2010, 'LCA allocation procedure used as an incitative method for waste recycling: An application to mineral additions in concrete', *Resources, Conservation and Recycling*, vol. 54, pp. 1231–1240.

Coates, J, 2000, 'Interpretation of infrared spectra, a practical approach', *Encyclopedia of Analytical Chemistry*, pp. 1-23.

Crossin, E, 2015, 'The greenhouse gas implications of using ground granulated blast furnace slag as a cement substitute', *Journal of Cleaner Production*, vol. 95, pp. 101-108.

Dai, B, Zhang, J 2012, 'The research of blast furnace slag fluidity by viscosity experiment and phase diagram analysis', *Metallurgical International*, vol. XVII, no. 6, pp. 25-28.

Dimitrova, S, 1995, 'Metal sorption on blast-furnace slag', *Water Research*, vol. 30, no. 1, pp. 228-232.

Dippenaar, R, 2005, 'Industrial uses of slag (the use and re-use of iron and steelmaking slags)', *Ironmaking & Steelmaking*, vol. 32, no.1, pp. 35-46.

Eisenhuttenleute, V, 1999, *Slag Atlas*, VerlagStahleisen, Dusseldorf, Germany.

Formoso, A, Babich, A, Gudenay, H, Garcia, A, Cores, A, 1999, 'Heat exchange in the hearth of a blast furnace operating with combined blast parameters', *ISIJ International*, vol. 39, no. 11, pp. 1134-1139.

Francis, A, 2005, 'Non-isothermal crystallization kinetics of a blast furnace slag glass', *Journal of the American Ceramic Society*, vol. 88, no. 7, pp.1859-1863.

Fredericci, C, Zanotto, E, Ziemath, E, 2000, 'Crystallization mechanism and properties of a blast furnace slag glass', *Journal of Non-Crystalline Solids*, vol. 273, pp. 64-75.

Gan, L, Lai, C, 2014, 'A general viscosity model for molten blast furnace slag', *Metallurgical and Materials Transactions* B, vol. 45B, pp. 875-888.

Grant, T, 2015, 'Life cycle inventory of cement & concrete produced in Australia', *Life Cycle Strategies Pty Ltd*, Melbourne, Australia.

Iron Ore & Global Market, 2015, Iron Ore Facts, viewed 16 December 2015, < http://www.ironorefacts.com/the-facts/iron-ore-global-markets>.

Ito,T, Yotsuji, J, Nagamune, A, 2014, 'Development of pig iron and molten slag level measurement technique for blast furnace', *ISIJ International*, vol. 54, no. 11, pp. 2618–2622.

Jak, E, Hayes, P, 2004, 'Phase equilibria determination in complex slag systems', paper presented at *International Conference on Molten Slags Fluxes and Salts, South African Institute of Mining and Metallurgy*.

Johansson, L, Gustafsson, J, 2000, 'Phosphate removal using blast furnace slag and Opoka-mechanisms', *Water Research*, vol. 34, no. 1, pp. 259-265.

Kan, T, Strezov, V, Evans, T, Nelson, P, 2015, 'Trace element deportment and particle formation behaviour during thermal processing of iron ore: technical reference for risk assessment of iron ore processing', *Journal of Cleaner Production*, vol. 102, pp. 384-393.

Kang, Y, Lee, J, Morita, K, 2014, 'Thermal conductivity of molten slags: a review of measurement techniques and discussion based on microstructural analysis', *ISIJ International*, vol. 54, no. 9, pp. 2008–2016.

Kim, J, Lee,Y, Min, D, Jung, S, Yi, S, 2004, 'Influence of MgO and Al_2O_3 contents on viscosity of blast furnace type slags containing FeO', *ISIJ International*, vol. 44, no. 8, pp. 1291–1297.

Kriskova, L, Pontikes, Y, Pandelaers, L, Cizer, O, Jones, P, Balen, K, Blanpain, B, 2013, 'Effect of high cooling rates on the mineralogy and hydraulic properties of stainless steel slags', *Metallurgical and Materials Transactions B*, vol. 44B, pp. 1173-1184.

Kumar, S, Kumar, R, Bandopadhyay, A, Alex, T, Kumar, B, Das, S, Mehrotra, S, 2008, 'Mechanical activation of granulated blast furnace slag and its effect on the properties and structure of Portland slag cement', *Cement & Concrete Composites*, vol. 30, pp. 679–685.

Kuo, Y, Wang, J, Wang, C, Tsai, C, 2008, 'Effect of water quenching and SiO_2 addition during vitrification of fly ash Part 1: On the crystalline characteristics of slags', *Journal of Hazardous Materials*, vol. 152, pp. 994–1001.

Lee, Y, Kim, J, Yi, S, Min, D, 2004, 'Viscous behaviour of CaO-SiO_2-Al_2O_3-MgO-FeO slag', VII *International Conference on Molten Slags Fluxes and Salts, The South African Institute of Mining and Metallurgy*.

Liang, X, Jin, Y, Wang, Y, 2011, 'Effect of additives on melting point and viscosity of rhrefining slag', *The Open Materials Science Journal*, vol. 5, pp. 9-14.

Liapis, I, Papayianni, I, 2015, 'Advances in chemical and physical properties of electric arc furnace carbon steel slag by hot stage processing and mineral mixing', *Journal of Hazardous Materials*, vol. 283, pp. 89–97.

Logachev, G, Gostenin, V, Pishnograev, S, Seleznev, D, Gridasov, V, 2013, 'Mobility of blast-furnace slag', *Steel in Translation*, vol.43, no. 12, pp. 805.-807.

Madejova, J, 2003, 'FTIR techniques in clay mineral studies', *Vibrational Spectroscopy*, vol. 31, pp. 1–10.

Memon, S, Loa, T, Barbhuiya, S, Xu, W, 2013, 'Development of form-stable composite phase change material byincorporation of dodecyl alcohol into ground granulated blast furnace', *Energy and Buildings*, vol. 62, pp. 360‑367.

Mendybaev, R, Richter, F, Davis, A, 2006, 'Reevaluation of the akermanite-gehlenite binary system', *37th Annual Lunar and Planetary Science Conference, March 13-17, 2006, League City, Texas*.

Menendez, G, Bonavetti, V, Irassar, E, 2003, 'Strength development of ternary blended cement with limestone filler and blast-furnace slag', *Cement & Concrete Composites*, vol. 25, pp. 61–67.

Meyer, C, 2009, 'The greening of the concrete industry', *Cement & Concrete Composites*, vol. 31, pp. 601‑605.

Motz, H, Geiseler, J, 2001, 'Products of steel slags an opportunity to save natural resources', *Waste Management*, vol. 21, pp. 285-293.

Nakamoto, M, Tanaka, T, Lee, J, Usui, T, 2004, 'Evaluation of viscosity of molten SiO_2–CaO–MgO–Al_2O_3slags in blast furnace operation', *ISIJ International*, vol. 44, no. 12, pp. 2115–2119.

National Slag Association, 2013, National Slag Association, viewed 1 March 2016, <http://www.nationalslag.org/blast-furnace-slag >.

Nazari, A, Riahi, S, 2011, 'The role of SiO_2 nanoparticles and ground granulated blast furnace slag admixtures on physical, thermal and mechanical properties of self-compacting concrete', *Materials Science and Engineering*, vol. 528, pp. 2149–2157.

Ngo, P, 1999, '*Failure Analysis of Integrated Circuits*, Springer, New York.

Ozturk, Z, Gultekin, E, 2015, 'Preparation of ceramic wall tiling derived from blast furnace slag', *Ceramics International*, vol. 41, pp. 12020–12026.

Park, H, Park, J, Kim, G, Shon, I 2012, 'Effect of TiO2 on the viscosity and slag structure in blast furnace type slags', *steel research int*., vol. 83, no. 2, pp. 150-156.

Podor, R, Ravaux, J, Brau, H, 2012, *In Situ Experiments in the Scanning Electron Microscope Chamber*, Scanning Electron Microscopy, <http://www.intechopen.com/books/scanning-electron-microscopy/in-situ-experiments-in-the-scanning-electron-microscope-chamber>.

PRe Sustainability, 2013, PRe Sustainability, viewed 29 February 2016, <https://www.pre-sustainability.com/simapro>.

Rumyantsev, Y, Fainer, N, Maximovskii, E, Ayupov, B, 2010, 'Elemental composition analysis silicon carbonitride thin films by energy dispersive spectroscopy', *Journal of Structural Chemistry*, vol. 51, pp. S179-S185.

Saito, N, Hori, N, Nakashima, K, Mori, K, 2003, 'Viscosity of blast furnace type slags', *Metallurgical and Materials Transactions B*, vol. 34B, pp. 509-516.

Savastano, H, Warden, P, Coutts, R, 2001, ' Ground iron blast furnace slag as a matrix for cellulose-cement materials', *Cement & Concrete Composition*, vol. 23, pp. 389-397.

Shen, M, Qiu, K, Zhang, L, Wang, Z, Liu, J, 2015, 'Influence of coal blending on ash fusibility in reducing atmosphere', *Energies*, vol. 8, pp. 4735-4754.

Strezov, V, 2006, 'Iron ore reduction using sawdust: experimental analysis and kinetic modelling', *Renewable Energy*, vol. 31, pp. 1892–1905.

Togobitskaya, D, Otorvin, P, Bel'kova, A Grin'ko, A, 2004, 'Automated system for monitoring and controlling the slag regime in blast furnace smelting', *Metallurgist*, vol. 48, pp.147-152.

U.S, Geological Survey, 2014, Data Market, viewed 12 November 2015, <https://datamarket.com/data/set/17b5/iron-and-steel-slag-end-use-statistics#!ds=17b5!kgu=2.f.g.8.b.i.j.9.a.d.c&display=line >.

Wan, H, Shui, A, Lin, Z, 2004, 'Analysis of geometric characteristics of GGBS particles and their influences on cement properties', *Cement and Concrete Research*, vol. 34, pp. 133–137.

Wang, Z, Ni, W, Jia, Y, Zhu, L, Huang, X, 2010, 'Crystallization behaviour of glass ceramics prepared from the mixture of nickel slag, blast furnace slag and quartz sand', *Journal of Non-Crystalline Solids*, vol. 356, pp. 1554–1558.

Yue, Y, Zhang, X, Xu, Y, Huang, S, Chen, P, 2014, 'Structural, dielectric and melting properties of aluminosilicate glasses based on blast furnace slag for printed circuit board applications', *Materials Letters*, vol. 136, pp. 356–358.

Zhao, H, Sun, W, Wu, X, Gao, B 2015, 'The properties of the self-compacting concrete with fly ash and ground granulated blast furnace slag mineral admixtures', *Journal of Cleaner Production*, vol. 95, pp. 66-74.

Zheng, K, Zhang, Z, Liu, L, Wang, X, 2014, 'Investigation of the viscosity and structural properties of CaO-SiO_2-TiO_2 slags', *Metallurgical and Materials Transactions B*, vol. 45B, pp. 1389-1397.